

Robust Nonlinear Data-Driven Predictive Control for Mixed Vehicle Platoons via Koopman Operator and Reachability Analysis

Shuai Li, Jiawei Wang, Kaidi Yang, Qing Xu, Jianqiang Wang, and Keqiang Li

Abstract— Mixed vehicle platoons, comprising connected and automated vehicles (CAVs) and human-driven vehicles (HDVs), hold significant potential for enhancing traffic performance. Most existing research assumes linear system dynamics and often ignores the impact of critical factors such as noise, disturbances, and attacks, which are inherent to real-world scenarios. To address these limitations, we propose a Robust Nonlinear Data-Driven Predictive Control (RNDDPC) framework that ensures safe and optimal control under uncertain and adverse conditions. By utilizing Koopman operator theory, we map the system’s nonlinear dynamics into a higher-dimensional space, constructing a Koopman-based linear predictor that approximates the behavior of the original nonlinear system. To mitigate modeling errors associated with this predictor, we introduce a data-driven reachable set analysis technique that performs secondary learning using matrix zonotope sets, generating a reachable set predictor for over-approximation of the future states of the underlying system. Then, we formulate the RNDDPC optimization problem and solve it in a receding horizon manner for robust control inputs. Extensive simulations demonstrate that the proposed framework significantly outperforms baseline methods in tracking performance under noise, disturbances, and attacks.

Index Terms—Mixed traffic, vehicle platoon, nonlinear data-driven control, robust control.

I. INTRODUCTION

WITH the rapid advancement of information and communication technologies, connected and automated vehicles (CAVs) have achieved significant progress in mass production and deployment, steadily gaining a growing share of the automotive market [1], [2]. As this trend continues, traffic systems are poised to transition into mixed traffic environments, where CAVs and human-driven vehicles (HDVs) coexist [3]–[5]. While these developments hold great potential for transforming transportation systems, ensuring driving safety and improving traffic efficiency in mixed traffic scenarios remain critical challenges [4], [6], [7]. Mixed vehicle platoons, comprising both CAVs and HDVs, have garnered increasing attention for their potential to address these challenges. The feasibility and effectiveness of such platoons have

been validated through traffic simulations [8], [9] and real-world experiments [10], [11].

Research on mixed vehicle platoon control strategies has primarily focused on model-based approaches, which rely on well-established car-following models to describe the behavior of HDVs. Commonly used models include the optimal velocity model (OVM) [12] and the intelligent driver model (IDM) [13]. These models provide the foundation for state-space representations of mixed vehicle platoons, enabling the design of various control strategies. Control techniques such as \mathcal{H}_∞ robust control [14], linear quadratic regulator [10], model predictive control (MPC) [3], and control barrier function [15] have been proposed to achieve optimal or near-optimal performance with theoretical guarantees. However, the performance of model-based strategies heavily depends on the accuracy of the underlying models. Accurately identifying parameters in these models, particularly for HDVs, poses a significant challenge and may limit the practical effectiveness of such control approaches.

In response to the limitations of model-based approaches, data-driven methods have gained increasing attention for their ability to bypass the explicit parameter identification required in system models. Among these methods, data-driven MPC integrates the established MPC framework with data-driven techniques, showing potential for achieving optimal control while respecting system constraints and maintaining stability guarantees [16]. One prominent example is the application of Data-Enabled Predictive Control (DeePC) [17] to mixed vehicle platoons. DeePC and its variants have been validated through simulation studies, showing their effectiveness in dampening traffic waves [9], reducing energy consumption [18], and protecting privacy safety [19]. However, deploying these strategies in real-world traffic scenarios faces several challenges. Noise inherent in onboard sensors and roadside perception systems can compromise data accuracy [20]. The dynamic and often unpredictable variations of the head vehicle’s velocity create mismatches between online predictions and actual traffic conditions [21]. Additionally, the adoption of Internet of Vehicles (IoV) technologies exposes CAV control systems to potential adversarial attacks, such as maliciously altered control inputs or manipulated sensor data [22], which could compromise safety. Despite these concerns, most existing studies fail to adequately account for the influence of noise in data collection and online control, oversimplistically assume constant head vehicle velocities, and neglect the risks posed by attacks. These simplifications can reduce trajectory tracking accuracy, weaken

This work is supported by National Natural Science Foundation of China with 52221005. Corresponding authors: Keqiang Li and Kaidi Yang.

S. Li, Q. Xu, J. Wang, and K. Li are with the School of Vehicle and Mobility, Tsinghua University, Beijing, China. (li-s21@mails.tsinghua.edu.cn, {qingxu, wjqlws, likq}@tsinghua.edu.cn).

J. Wang is with the Department of Civil and Environmental Engineering, University of Michigan, Ann Arbor, USA. (jiawe@umich.edu).

K. Yang is with the Department of Civil and Environmental Engineering, National University of Singapore, Singapore. (ykaidi@nus.edu.sg).

robustness, and increase safety risks in mixed vehicle platoon control.

Recent studies have made significant progress in enhancing the robustness of mixed vehicle platoon systems. For instance, reformulating the DeePC framework using min-max robust optimization has been shown to mitigate the impact of unknown disturbances originating from the head vehicle [21]. A distributed data-driven MPC approach with feedforward compensation has also effectively countered external disturbances [23]. Additionally, zonotopic data-driven predictive control (ZPC), which utilizes linear reachability analysis, has successfully minimized the influence of observational noise on data collection [20]. While these approaches enhance robustness, they exhibit certain limitations. Under noise-free conditions, the DeePC predictor established in [21] has been proven to be equivalent to the linear MPC formulation for linear time-invariant (LTI) systems [17], [24]. Similarly, the subspace identification matrix generation in [23] depends on the assumption of linearity, and the reachability set computation in [20] also relies on the properties of linear systems. In practice, mixed vehicle platoons exhibit strongly nonlinear behavior, particularly in human driver responses. The aforementioned methods do not fully capture these nonlinear dynamics, limiting their effectiveness in real-world applications.

To address these gaps concerning robustness and nonlinearity in mixed vehicle platoons, we propose a Robust Nonlinear Data-Driven Predictive Control (RNDDPC) framework that integrates Koopman operator theory and reachability analysis. Specifically, considering the nonlinear nature of mixed vehicle platoons, inspired by [25]–[27], we employ Koopman operator theory to represent the nonlinear system as a high-dimensional linear system. Based on the extended dynamic mode decomposition (EDMD) method [28], we effectively utilize deep neural networks (DNN) to learn and construct a Koopman-based linear predictor that approximates the dynamics of the original nonlinear system. Notably, unlike previous methods [25]–[27] directly applies the Koopman-based linear predictor for control, the proposed method explicitly addresses the challenges arising from noise, disturbances, and attacks in real-world applications. To enhance robustness, we introduce a data-driven reachability analysis method, utilizing matrix zonotope sets to perform secondary learning and generate a robust reachable set predictor. This predictor over-approximates the system’s future states, accounting for uncertainties and ensuring robust predictions under various conditions. Within a receding horizon manner, we formulate and solve the RNDDPC optimization problem with safety constraints to compute robust control inputs. This enables the development of a robust data-driven predictive control strategy for nonlinear mixed vehicle platoons, ensuring system safety against uncertainties and unfavorable conditions. Precisely, the key contributions of this work are as follows:

- 1) We introduce a deep EDMD method for modeling mixed vehicle platoons. Unlike previous work [20], [21], [23] that relies on linear assumptions, our approach explicitly captures the nonlinear characteristics of the system. By utilizing actual measurement data, the proposed method approximates the lifting function via DNN, generating

a high-dimensional Koopman-based linear model that effectively represents the dynamics of mixed vehicle platoons. This eliminates the need for explicit model knowledge, which is often required by methods [3], [10], [14], [15]. The linearity of the Koopman-based model facilitates controller design using well-established linear system theory, offering a more efficient and interpretable solution compared to complex nonlinear modeling strategies or less transparent reinforcement learning techniques.

- 2) We propose a RNDDPC method for mixed vehicle platoons. Unlike previous approaches [25]–[27] that directly apply the Koopman-based model for control design, our method addresses modeling errors caused by noise and inaccuracies. To enhance robustness, we utilize matrix zonotope set technology for secondary learning, constructing an over-approximated set of system models. Additionally, we account for potential disturbances and attacks by defining them as zonotope sets, rather than assuming them to be zero as in [9]. For each control horizon, we formulate a data-driven reachable set predictor using matrix zonotope set technology and design an RNDDPC optimization problem to ensure that the predicted states always satisfy safety constraints, achieving safe and optimal control for CAVs.
- 3) We extensively evaluate the effectiveness of the proposed RNDDPC method through extensive simulations, with a particular focus on its robustness against noise, disturbances, and attacks. A comparative analysis is conducted with multiple baseline approaches, including linear MPC, nonlinear MPC, Koopman MPC [26], [27], DeePC [9], [17], and ZPC [20], [29]. The simulation results indicate that, compared to all baselines, RNDDPC significantly reduces the tracking velocity mean error, tracking spacing mean error, and total real cost in both comprehensive and emergency scenarios. These results highlight the enhanced robustness and tracking accuracy of the RNDDPC method for controlling mixed vehicle platoons, particularly in the presence of adverse conditions.

The rest of this paper is organized as follows. Section II provides the foundational preliminaries. Section III presents data-driven modeling of mixed vehicle platoon systems. Section IV introduces the formulation of the proposed RNDDPC framework. Numerical simulations are provided in Section V, and Section VI concludes this paper.

II. PRELIMINARIES

This section presents the essential preliminaries on reachable sets for data-driven predictive control. For clarity and conciseness, we may slightly abuse some notations, which will be defined specifically for use within this section. Inspired by [20], [22], [30], we adopt zonotope sets to represent reachable sets, ensuring computational efficiency. The key definitions and set representations relevant to reachable set computations are outlined below.

Definition 1 (Interval Set [31]): An interval set \mathcal{H} is a connected subset of \mathbb{R}^n , and it can be defined as $\mathcal{H} = \{x_{\mathcal{H}} \in \mathbb{R}^n \mid \underline{x}_{\mathcal{H}_i} \leq x_{\mathcal{H}_i} \leq \bar{x}_{\mathcal{H}_i}, \forall i = 1, \dots, n\}$, where

$\underline{x}_{\mathcal{H}_i}$ and $\bar{x}_{\mathcal{H}_i}$ are the lower bound and upper bound of $x_{\mathcal{H}_i}$, respectively. Interval set can be represented as $\mathcal{H} = [\underline{\mathcal{H}}, \bar{\mathcal{H}}]$, with $\underline{\mathcal{H}} = [\underline{x}_{\mathcal{H}_1}, \underline{x}_{\mathcal{H}_2}, \dots, \underline{x}_{\mathcal{H}_n}]$ and $\bar{\mathcal{H}} = [\bar{x}_{\mathcal{H}_1}, \bar{x}_{\mathcal{H}_2}, \dots, \bar{x}_{\mathcal{H}_n}]$.

Definition 2 (Zonotope Set [32]): Given a center vector $c_{\mathcal{Z}} \in \mathbb{R}^n$, and $\gamma_{\mathcal{Z}} \in \mathbb{N}$ generator vectors in a generator matrix $G_{\mathcal{Z}} = [g_{\mathcal{Z}}^{(1)}, g_{\mathcal{Z}}^{(2)}, \dots, g_{\mathcal{Z}}^{(\gamma_{\mathcal{Z}})}] \in \mathbb{R}^{n \times \gamma_{\mathcal{Z}}}$, a zonotope set is defined as $\mathcal{Z} = \langle c_{\mathcal{Z}}, G_{\mathcal{Z}} \rangle = \{x \in \mathbb{R}^n \mid x = c_{\mathcal{Z}} + \sum_{i=1}^{\gamma_{\mathcal{Z}}} \beta^{(i)} g_{\mathcal{Z}}^{(i)}, -1 \leq \beta^{(i)} \leq 1\}$. For zonotope sets, the following operations hold:

- **Linear Map:** For a zonotope set $\mathcal{Z} = \langle c_{\mathcal{Z}}, G_{\mathcal{Z}} \rangle$, $L \in \mathbb{R}^{m \times n}$, the linear map is defined as $L\mathcal{Z} = \langle Lc_{\mathcal{Z}}, LG_{\mathcal{Z}} \rangle$.
- **Minkowski Sum:** Given two zonotope sets $\mathcal{Z}_1 = \langle c_{\mathcal{Z}_1}, G_{\mathcal{Z}_1} \rangle$ and $\mathcal{Z}_2 = \langle c_{\mathcal{Z}_2}, G_{\mathcal{Z}_2} \rangle$ with compatible dimensions, the Minkowski sum is defined as $\mathcal{Z}_1 + \mathcal{Z}_2 = \langle c_{\mathcal{Z}_1} + c_{\mathcal{Z}_2}, [G_{\mathcal{Z}_1}, G_{\mathcal{Z}_2}] \rangle$.
- **Cartesian Product:** Given two zonotope sets $\mathcal{Z}_1 = \langle c_{\mathcal{Z}_1}, G_{\mathcal{Z}_1} \rangle$ and $\mathcal{Z}_2 = \langle c_{\mathcal{Z}_2}, G_{\mathcal{Z}_2} \rangle$, the cartesian product is defined as

$$\mathcal{Z}_1 \times \mathcal{Z}_2 = \left\langle \begin{bmatrix} c_{\mathcal{Z}_1} \\ c_{\mathcal{Z}_2} \end{bmatrix}, \begin{bmatrix} G_{\mathcal{Z}_1} & 0 \\ 0 & G_{\mathcal{Z}_2} \end{bmatrix} \right\rangle. \quad (1)$$

- **Over-approximation:** A zonotope set $\mathcal{Z} = \langle c_{\mathcal{Z}}, G_{\mathcal{Z}} \rangle$ could be over-approximated by an interval set denoted as Definition 1 with operation is defined as

$$\mathcal{H} = \text{interval}(\mathcal{Z}) = [c_{\mathcal{Z}} - \Delta g_{\mathcal{Z}}, c_{\mathcal{Z}} + \Delta g_{\mathcal{Z}}], \quad (2)$$

where $\Delta g_{\mathcal{Z}} = \sum_{i=1}^{\gamma_{\mathcal{Z}}} |g_{\mathcal{Z}}^{(i)}|$, with the absolute value is taken element-wise.

Definition 3 (Matrix Zonotope Set [31]): Given a center matrix $C_{\mathcal{M}} \in \mathbb{R}^{n \times m}$, and $\gamma_{\mathcal{M}} \in \mathbb{N}$ generator matrices in a generator matrix $G_{\mathcal{M}} = [g_{\mathcal{M}}^{(1)}, g_{\mathcal{M}}^{(2)}, \dots, g_{\mathcal{M}}^{(\gamma_{\mathcal{M}})}] \in \mathbb{R}^{n \times m \gamma_{\mathcal{M}}}$, a matrix zonotope set is defined as $\mathcal{M} = \langle C_{\mathcal{M}}, G_{\mathcal{M}} \rangle = \{X \in \mathbb{R}^{n \times m} \mid X = C_{\mathcal{M}} + \sum_{i=1}^{\gamma_{\mathcal{M}}} \beta^{(i)} G_{\mathcal{M}}^{(i)}, -1 \leq \beta^{(i)} \leq 1\}$.

III. DATA-DRIVEN MODELING OF MIXED VEHICLE PLATOON SYSTEM

This section introduces the problem statement, presents the basic parametric nonlinear model of the mixed vehicle platoon system, and discusses the data-driven modeling approach using the Koopman operator theory.

A. Problem Statement

We consider a mixed vehicle platoon system consisting of one leading CAV (indexed as 1) and $n - 1$ following HDVs (indexed as 2, ..., n), as depicted in Fig. 1. The set of all vehicle indices in the platoon is denoted as $\Omega = \{1, 2, \dots, n\}$, where $\Omega_C = \{1\}$ and $\Omega_H = \{2, \dots, n\}$ represent the indices of the CAV and the HDVs, respectively. The entire platoon follows a head vehicle (indexed as 0), which is positioned immediately ahead of the mixed vehicle platoon. This configuration is called the Leading Cruise Control (LCC) in [33].

As depicted in Fig. 1, this study introduces a centralized control framework designed to optimize the operation of a mixed vehicle platoon in real-time, leveraging the substantial

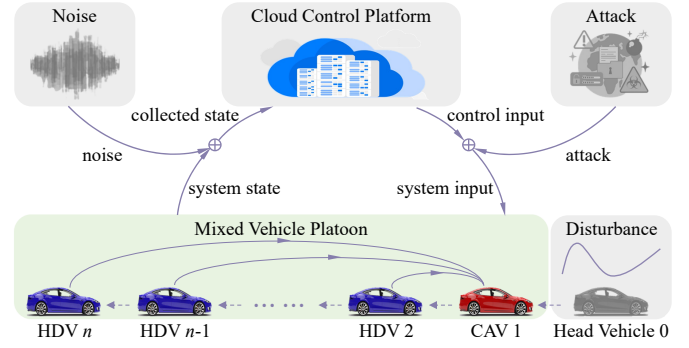


Fig. 1. The schematic of the mixed vehicle platoon consists of a leading CAV (red) and multiple following HDVs (blue), following behind a head vehicle (gray). The green box represents the mixed vehicle platoon. The disturbance originates from variations in the head vehicle's velocity. The noise and attacks affect the uplink and downlink of the cloud control platform, respectively.

computing capabilities of a cloud control platform. Specifically, the cloud platform is assumed to collect real-time data seamlessly from all vehicles in the platoon. Based on this data, the centralized controller generates control commands, which are transmitted to the CAV to regulate its behavior and influence the entire platoon.

The management of mixed vehicle platoons presents significant challenges due to the inherent human-in-the-loop interactions and the nonlinear dynamics of the system. These challenges are further compounded by external factors, including noise in state observations, disturbances from variations in the head vehicle's velocity, and potential adversarial attacks on the control inputs of the CAV. In such complex scenarios, the challenge is to control the CAV effectively while ensuring that the following HDVs adjust their velocities in a coordinated manner. This is essential to guarantee safe operation under various driving conditions.

To address these challenges, this paper focuses on developing a robust nonlinear data-driven control framework that effectively addresses the complex nonlinear dynamics inherent in mixed vehicle platoons, while mitigating the impact of noise, disturbances, and attacks. The proposed strategy aims to enhance the safety and stability of the mixed vehicle platoon, providing a novel and practical solution for real-world applications.

B. Parametric Modeling for Nonlinear Dynamics

In this part, we introduce the parametric model of the mixed vehicle platoon system. For each vehicle $i \in \Omega$, the longitudinal dynamics are modeled using a second-order system [33]–[35]:

$$\begin{cases} p_i(k+1) = p_i(k) + t_s v_i(k), \\ v_i(k+1) = v_i(k) + t_s u_i(k), \end{cases} \quad i \in \Omega \quad (3)$$

where $p_i(k)$ and $v_i(k)$ represent the position and velocity of vehicle i at the discrete time step k , $u_i(k)$ denotes the control input (acceleration), and t_s is the sampling time.

For HDVs, the control input $u_i(k)$ is typically determined by the driver and is modeled using widely accepted car-

following models, such as the OVM [12] and IDM [13]. The general discrete form of these models can be expressed as:

$$u_i(k) = F_i(s_i(k), v_i(k), v_{i-1}(k)), \quad i \in \Omega_H \quad (4)$$

where $s_i(k) = p_{i-1}(k) - p_i(k)$ denotes the spacing between vehicle i and its preceding vehicle $i-1$, and $F_i(\cdot)$ is a nonlinear function capturing the behavior of the HDV.

By combining (3) and (4), and selecting $s_i(k)$ and $v_i(k)$ as the state variables, the state-space representation of the HDVs can be derived as:

$$\begin{cases} s_i(k+1) = s_i(k) + t_s(v_{i-1}(k) - v_i(k)), \\ v_i(k+1) = v_i(k) + t_s F_i(s_i(k), v_i(k), v_{i-1}(k)). \end{cases} \quad i \in \Omega_H \quad (5)$$

For CAVs, we assume that the control input is subject to adversarial attacks, similar to the HDVs model (5), the longitudinal dynamics of CAVs can be expressed as follows:

$$\begin{cases} s_i(k+1) = s_i(k) + t_s(v_{i-1}(k) - v_i(k)), \\ v_i(k+1) = v_i(k) + t_s u(k) + t_s \vartheta(k), \end{cases} \quad i \in \Omega_C \quad (6)$$

where $u(k)$ represents the designed control input for the CAV, and $\vartheta(k)$ captures the adversarial attacks for control input, adhering to the bounded condition $|\vartheta(k)| \leq \vartheta_{\max} \in \mathbb{R}$. The modeling of such attacks is discussed in [22], [36].

We define the state vector for each vehicle i as $x_i(k) = [s_i(k), v_i(k)]^\top$. By combining the state vectors of all vehicles $i \in \Omega$ in the mixed vehicle platoon, the overall system state at time step k is given by:

$$x(k) = [x_1^\top(k), x_2^\top(k), \dots, x_n^\top(k)]^\top \in \mathbb{R}^{2n}. \quad (7)$$

Inspired by [20], [25], [33], [34], HDVs are treated as uncontrolled agents, while CAVs are modeled as agents under direct control. Based on (5)-(7) and accounting for the influence of noise, we formulate the nonlinear model of the mixed vehicle platoon system as follows:

$$x(k+1) = f(x(k), u(k), \epsilon(k), \vartheta(k)) + \omega(k), \quad (8)$$

where $f(\cdot)$ denotes the nonlinear dynamics, and $u(k) \in \mathbb{R}$, $\epsilon(k) = v_0(k) \in \mathbb{R}$, $\vartheta(k) \in \mathbb{R}$, and $\omega(k) \in \mathbb{R}^{2n}$ denote the control input of the CAV, the external disturbance (head vehicle velocity), the adversarial attacks, and the unknown but bounded noise, meeting the bounded condition $|\omega(k)| \leq \omega_{\max} \in \mathbb{R}^{2n}$, respectively.

Remark 1: The nonlinear behavior and uncertainties inherent in HDVs complicate the accurate modeling and control of the mixed vehicle platoon system described in (8). These challenges necessitate the development of a data-driven predictive control method to determine the optimal control input $u(k)$ for the CAV. We use the parametric nonlinear model in (8) to clarify the dimensions and physical significance of state and control variables, which is crucial for the design of data-driven control discussed in Section IV.

C. Preliminary Data-Driven Modeling by Koopman Operator

The Koopman operator framework effectively captures the essential characteristics of nonlinear systems by transforming

them into a higher-dimensional space, where their dynamics can be described linearly [26], [27]. For the nonlinear system (8) with noise set to zero ($\omega(k) = 0$), the dynamics are expressed as follows:

$$x(k+1) = f(x(k), u(k), \epsilon(k), \vartheta(k)). \quad (9)$$

We extend the state space by taking the product of the original state space and the space of all possible control sequences, following the rigorous and practical method in [26]. Specifically, the extended state is defined as:

$$\chi(k) = \begin{bmatrix} x(k) \\ \mathbf{u} \\ \epsilon \\ \vartheta \end{bmatrix}, \quad (10)$$

where $\chi(k)$ denotes the extended state, $\mathbf{u} := \{u(k)\}_{k=0}^\infty$ represents an infinite sequence of control inputs, $\epsilon := \{\epsilon(k)\}_{k=0}^\infty$ denotes an infinite sequence of disturbances, and $\vartheta := \{\vartheta(k)\}_{k=0}^\infty$ indicates an infinite sequence of attacks.

Then, the system dynamics (8) can be reformulated as:

$$\chi(k+1) = F(\chi(k)) = \begin{bmatrix} f(x(k), u(k), \epsilon(k), \vartheta(k)) \\ \mathcal{S}\mathbf{u} \\ \mathcal{S}\epsilon \\ \mathcal{S}\vartheta \end{bmatrix}, \quad (11)$$

where $F(\cdot)$ defines the extended system dynamics, and \mathcal{S} denotes the left shift operator, defined as $\mathcal{S}u(k) := u(k+1)$, $\mathcal{S}\epsilon(k) := \epsilon(k+1)$, and $\mathcal{S}\vartheta(k) := \vartheta(k+1)$.

In this way, the Koopman operator $\mathcal{K} : \mathcal{H} \rightarrow \mathcal{H}$ for the extended system described by (11) is defined as [26]:

$$\mathcal{K}\Theta(\chi(k)) = \Theta(F(\chi(k))) = \Theta(\chi(k+1)), \quad (12)$$

where lifting function $\Theta(\chi(k))$ belongs to the extended lifting space \mathcal{H} , which is a higher-dimensional space that transforms the original state variables, such as $x(k)$, \mathbf{u} , ϵ , and ϑ , into new features or functions.

It is important to note that the system model in (12) represents a linear operator that effectively characterizes the nonlinear dynamics of the system (8). However, the Koopman operator \mathcal{K} generally exists in an infinite-dimensional space, which arises from the infinite-dimensional nature of the variable $\chi(k)$ in (10), which presents significant computational challenges.

Inspired by the EDMD method [26], [28], we approximate the infinite-dimensional Koopman operator \mathcal{K} with a finite-dimensional operator $\mathcal{K}_{n_\psi} \in \mathbb{R}^{n_\psi \times n_\psi}$, where n_ψ represents the dimension of the Koopman operator approximation. Specifically, the EDMD method involves constructing a dataset $\{\chi(k)\}_{1:N_c}$, which is sampled independently according to a non-negative probability distribution that satisfies (11), where n_c denotes the number of collected data points. The finite-dimensional approximation \mathcal{K}_{n_ψ} is then computed by solving the following optimization problem:

$$\min_{\mathcal{K}_{n_\psi}} \sum_{j=1}^{n_c-1} \left\| \Psi(\chi(k+1)) - \mathcal{K}_{n_\psi} \Psi(\chi(k)) \right\|_2^2, \quad (13)$$

where $\Psi(\chi(k)) = [\psi_1(\chi(k)), \psi_2(\chi(k)), \dots, \psi_{n_\psi}(\chi(k))]^\top$ denotes a vector of lifting functions, with $\psi_i(\chi(k))$ representing the i -th basis function for $i \in \{1, 2, \dots, n_\psi\}$.

To enhance the computational feasibility of the Koopman operator, we select $\Psi(\chi(k))$ in (13) as follows:

$$\Psi(\chi(k)) = \begin{bmatrix} \Phi(x(k)) \\ u(k) \\ \epsilon(k) \\ \vartheta(k) \end{bmatrix}, \quad (14)$$

where $\Phi(x(k)) = [\phi_1(x(k)), \phi_2(x(k)), \dots, \phi_{n_\phi}(x(k))]^\top$, with $n_\phi > 2n$, ensuring that $n_\psi = n_\phi + 3$.

Then, we represent the first n_ϕ rows of \mathcal{K}_{n_ψ} as $[A \ B \ H \ J] \in \mathbb{R}^{n_\phi \times (n_\phi + 3)}$, where $A \in \mathbb{R}^{n_\phi \times n_\phi}$, $B \in \mathbb{R}^{n_\phi}$, $H \in \mathbb{R}^{n_\phi}$, and $J \in \mathbb{R}^{n_\phi}$ are the system matrix, control input matrix, disturbance input matrix, and attack input matrix, respectively. The matrices A , B , H , and J can be estimated using the data pairs $\{[x(k), u(k), \epsilon(k), \vartheta(k)]_{1:N_d}\}$ by solving the least squares problem as follows [26]:

$$\min_{A, B, H, J} \sum_{k=1}^{n_c-1} \|\Phi(x(k+1)) - \Xi\|_2^2, \quad (15)$$

where $\Xi = A\Phi(x(k)) + Bu(k) + H\epsilon(k) + J\vartheta(k)$.

To reconstruct $x(k)$ from $\Phi(x(k))$, the linear mapping matrix $C \in \mathbb{R}^{2n \times n_\phi}$ is obtained by solving [26]:

$$\min_C \sum_{k=1}^{n_c-1} \|x(k) - C\Phi(x(k))\|_2^2, \quad (16)$$

where C is a projection matrix from the lifting space into the original state space.

By solving (15) and (16) and defining the lifting state $z(k) = \Phi(x(k))$, the linear Koopman predictor for (8) is expressed as:

$$\begin{cases} z(k+1) = Az(k) + Bu(k) + H\epsilon(k) + J\vartheta(k), \\ x(k) = Cz(k). \end{cases} \quad (17)$$

Accordingly, the nonlinear mixed vehicle platoon system (8) with zero noise ($\omega(k) = 0$) has been approximately transformed into a high-dimensional linear system (17) via the Koopman operator.

Remark 2: The Koopman lifting system model in (17), derived using the Koopman operator, provides a linear approximation of the original nonlinear dynamics in (8). This linearization facilitates the formulation and solution of predictive control optimization problems. However, the presence of noise in (8) and the adoption of a finite-dimensional lifting function in (13) can lead to modeling errors. As discussed in the context of Koopman's fundamental theory in [37], [38], these modeling errors may degrade the performance of closed-loop control systems. Existing methods have not fully addressed these modeling inaccuracies [26], [27]. To overcome this issue, we further propose a robust nonlinear data-driven predictive control strategy that leverages the Koopman operator and reachability analysis, as detailed in Section IV.

IV. ROBUST NONLINEAR DATA-DRIVEN PREDICTIVE CONTROL FOR MIXED VEHICLE PLATOONS

In this section, we propose a Robust Nonlinear Data-Driven Predictive Control (RNDDPC) framework, which integrates the Koopman operator and reachability analysis, as illustrated in Fig. 2. Precisely, the RNDDPC framework is structured into three main phases:

1) **Data Collection Phase:** This phase involves gathering data that are essential for the control framework. The dataset comprises the control inputs $u(k)$ for the CAV, the disturbance inputs $\epsilon(k)$ from the head vehicle, the attack inputs $\vartheta(k)$, and the system state $x(k)$ of the mixed vehicle platoon system. All data are collected under the influence of noise $\omega(k)$, which is, however, not directly measurable (see Section IV-A).

2) **Offline Learning Phase:** Using the collected data, deep neural networks (DNNs) are trained to approximate the lifting function $\Phi(x(k))$. This lifting function is then utilized to construct matrix zonotope sets, \mathcal{M}_{ABHJ} and \mathcal{M}_C , through secondary learning, to model the unknown and uncertain dynamics of the mixed vehicle platoon system. These matrix zonotope sets serve as over-approximations of $[A \ B \ H \ J]$ and C in the linear Koopman predictor (17), effectively capturing the uncertain dynamics of the mixed vehicle platoon. The learned \mathcal{M}_{ABHJ} and \mathcal{M}_C are subsequently utilized during the online control phase to calculate the data-driven reachable set (see Section IV-B).

3) **Online Control Phase:** Using the learned matrix zonotope sets \mathcal{M}_{ABHJ} and \mathcal{M}_C , we recursively calculate the over-approximated data-driven reachable set of system states over the control horizon. The reachable set captures all potential states that the system can reach, accounting for modeling errors, disturbances, and adversarial attacks. This ensures a robust representation of system behavior. To improve computational efficiency, the zonotope-type reachable sets are approximated as interval-type reachable sets, providing upper and lower bounds for each state. By ensuring that these interval bounds stay within predefined safety constraints, a convex optimization problem is formulated for the RNDDPC approach. This problem is solved using a receding horizon control strategy to determine the optimal control input for the CAVs, ensuring safe operation even in the presence of noise, disturbances, and attacks (see Section IV-C).

A. Data Collection Phase

In this study, offline data are collected by applying control inputs to the CAVs, disturbance inputs to the head vehicle, and attack inputs to the CAVs, thereby exciting the mixed vehicle platoon system. As described by the parametric model of the mixed vehicle platoon system (8), it is evident that the system state $x(k)$ is influenced by the control input $u(k)$, the disturbance inputs $\epsilon(k)$, the attack input $\vartheta(k)$, and the noise $\omega(k)$. During the data collection process, $u(k)$, $\epsilon(k)$, and $\vartheta(k)$ are manually specified, and the system states $x(k)$ are directly measurable. Recall that, although the noise $\omega(k)$ is unknown, it is assumed to be bounded. To ensure the data adequately captures the system's dynamic characteristics, persistently exciting input sequences $u(k)$, $\epsilon(k)$, and $\vartheta(k)$ of

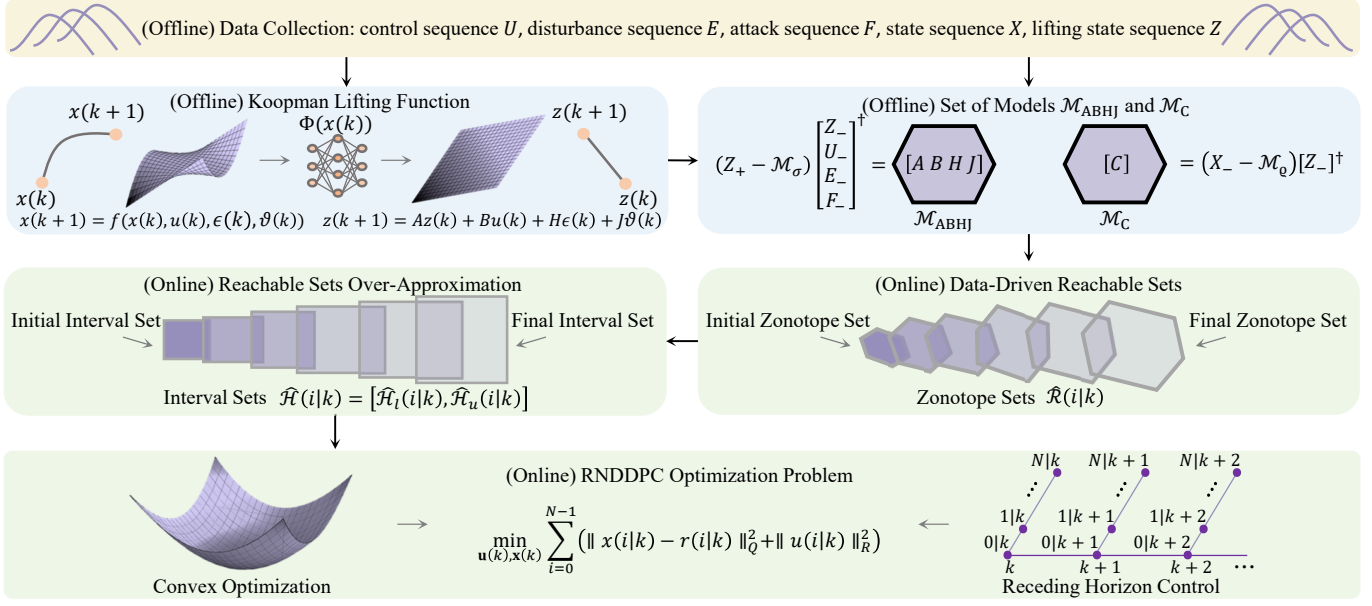


Fig. 2. The schematic of the proposed RNDDPC method for mixed vehicle platoons. In the offline learning phase (blue), pre-collected data (yellow) is utilized to train a deep neural network (DNN) that learns the lifting function $\Phi(x(k))$. Using $\Phi(x(k))$, this phase then computes over-approximated matrix zonotope sets \mathcal{M}_{ABHJ} and \mathcal{M}_C , corresponding to the Koopman system matrices $[A \ B \ H \ J]$ and C , respectively. In the online control phase (green), the RNDDPC framework focuses on determining a robust optimal control input. Specifically, it utilizes the matrix zonotope sets \mathcal{M}_{ABHJ} and \mathcal{M}_C to perform an online recursive computation of the data-driven reachable set for the system states, represented as zonotopes. To enhance computational efficiency, the zonotope-type reachable sets are approximated as interval-type reachable sets, providing straightforward upper and lower bounds for each state variable. Based on these interval bounds and predefined safety constraints, a convex optimization problem is formulated within the RNDDPC framework. This optimization problem is solved using a receding horizon control strategy, ensuring that the computed control input for the CAV maintains robust and safe operation in real-time.

length $T+1$ are applied to the system. Specifically, the control input sequence U , the disturbance input sequence E , the attack input sequence F , and the corresponding state sequence X are defined as follows:

$$U = [u(1), u(2), \dots, u(T+1)] \in \mathbb{R}^{1 \times (T+1)}, \quad (18a)$$

$$E = [\epsilon(1), \epsilon(2), \dots, \epsilon(T+1)] \in \mathbb{R}^{1 \times (T+1)}, \quad (18b)$$

$$F = [\vartheta(1), \vartheta(2), \dots, \vartheta(T+1)] \in \mathbb{R}^{1 \times (T+1)}, \quad (18c)$$

$$X = [x(1), x(2), \dots, x(T+1)] \in \mathbb{R}^{2n \times (T+1)}. \quad (18d)$$

Using $\Phi(x(k))$ from (14) and the state sequence X in (18d), we can obtain the lifting state sequence Z of states $z(k)$ in the Koopman lifting system model (17):

$$Z = [z(1), z(2), \dots, z(T+1)] \in \mathbb{R}^{n_\phi \times (T+1)}. \quad (19)$$

Next, all these collected or computed data are processed into standardized formats, which are then used to construct the matrix zonotope sets \mathcal{M}_{ABHJ} and \mathcal{M}_C for reachable set computation, as illustrated in Fig. 2. Specifically, the data sequences are reorganized as follows:

$$U_- = [u(1), u(2), \dots, u(T)] \in \mathbb{R}^{1 \times T}, \quad (20a)$$

$$E_- = [\epsilon(1), \epsilon(2), \dots, \epsilon(T)] \in \mathbb{R}^{1 \times T}, \quad (20b)$$

$$F_- = [\vartheta(1), \vartheta(2), \dots, \vartheta(T)] \in \mathbb{R}^{1 \times T}, \quad (20c)$$

$$X_- = [x(1), x(2), \dots, x(T)] \in \mathbb{R}^{2n \times T}, \quad (20d)$$

$$X_+ = [x(2), x(3), \dots, x(T+1)] \in \mathbb{R}^{2n \times T}, \quad (20e)$$

$$Z_- = [z(1), z(2), \dots, z(T)] \in \mathbb{R}^{n_\phi \times T}, \quad (20f)$$

$$Z_+ = [z(2), z(3), \dots, z(T+1)] \in \mathbb{R}^{n_\phi \times T}. \quad (20g)$$

B. Offline Learning Phase

In the offline learning phase, we utilize the pre-collected data to train a DNN to learn the lifting function, which enables us to approximate the nonlinear dynamics of the mixed vehicle platoon system within a higher-dimensional space. Based on this lifting function, we then construct over-approximated matrix zonotope sets \mathcal{M}_{ABHJ} and \mathcal{M}_C through secondary learning, to model the unknown and uncertain dynamics of the mixed vehicle platoon system. These matrix zonotope sets \mathcal{M}_{ABHJ} and \mathcal{M}_C play a critical role in the online control phase, as discussed in Section IV-C.

1) *Deep Neural Network Lifting Function*: To derive high-quality matrices A , B , H , J , and C for the linear Koopman lifting system (17), which characterizes the nonlinear dynamics in (8), a key challenge is the selection of the appropriate lifting function $\Phi(x(k))$ in (14). While common choices include radial basis functions, polynomials functions, and Gauss functions, determining the optimal lifting function remains an open research problem [39], [40]. To tackle this challenge, we employ the deep EDMD algorithm for modeling mixed vehicle platoon systems, where DNN is employed to automatically construct the lifting function $\Phi(x(k))$.

Following the method in [40], the lifting functions $\Phi(x(k))$ in (14) at time step k are formulated as:

$$\Phi(x(k)) = \begin{bmatrix} x(k) \\ g(x(k)) \end{bmatrix}, \quad (21)$$

where $x(k)$ represents the system state as given in (7), corresponding to the first $2n$ basis functions of $\Phi(x(k))$, denoted by $x(k) = [\phi_1(x(k)), \phi_2(x(k)), \dots, \phi_{2n}(x(k))]^\top$. The

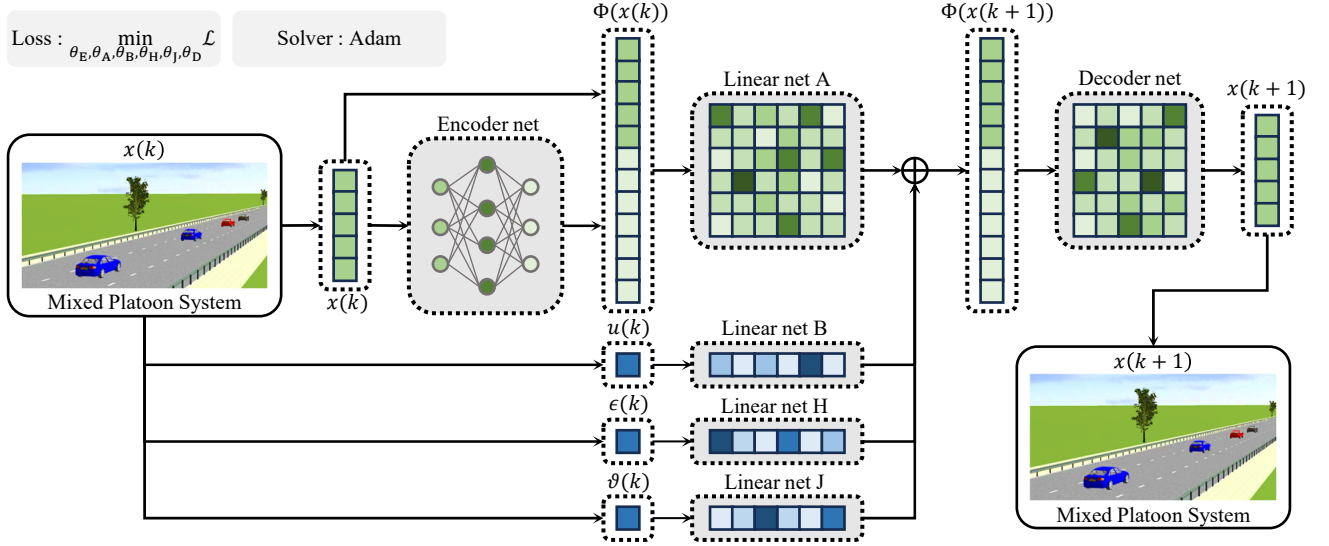


Fig. 3. The overview of the DNN framework for the deep EDMD learning approach. The original state $x(k)$ of the mixed vehicle platoon is lifted using both the state itself and an encoder net to obtain the lifting state $\Phi(x(k))$, referred to as $z(k)$. The lifting state $\Phi(x(k))$, along with the control input $u(k)$, disturbance input $\epsilon(k)$, and attack input $\vartheta(k)$ together construct a linear evolution in the lifting space, which generates the next lifting state $\Phi(x(k+1))$. The corresponding original state $x(k+1)$ of the mixed vehicle platoon is then reconstructed from the lifting state space via the decoder net. The lifting function $\Phi(x(k))$ is derived through automated training of the DNN, guided by a well-designed loss function.

remaining $n_\phi - 2n$ basis functions, represented as $g(x(k)) = [\phi_{2n+1}(x(k)), \phi_{2n+2}(x(k)), \dots, \phi_{n_\phi}(x(k))]^\top$, are learned by the encoder net. The architecture of the DNN is illustrated in Fig. 3, comprising three main components: an encoder net, a linear net, and a decoder net.

Encoder Net: The encoder net maps the system state $x(k)$ to a high-dimensional space $g(x(k))$, which consists of $n_\phi - 2n$ basis functions. This net is constructed as a multi-layer perceptron with n_e fully connected layers. For any hidden layer $p \in \{1, 2, \dots, n_e\}$, the output is defined as follows:

$$o_e^{(p)} = \sigma_e^{(p)} \left(W_e^{(p)} o_e^{(p-1)} + b_e^{(p)} \right), \quad (22)$$

where $o_e^{(p)}$ and $o_e^{(p-1)}$ represent the output and input of layer p , respectively. The activation function for layer p is $\sigma_e^{(p)}$. The weight matrix $W_e^{(p)} \in \mathbb{R}^{n_p \times n_{p-1}}$ and the bias vector $b_e^{(p)} \in \mathbb{R}^{n_p}$ are associated with layer p , where n_p is the number of neurons in layer p . The encoder network takes $o_e^{(0)} = x(k)$ as input and produces $o_e^{(n_e)} = g(x(k))$ as output. Rectified linear unit (ReLU) activations are applied to the layers for $p \in \{1, 2, \dots, n_e - 1\}$, while the final layer does not utilize activations. By combining the state $x(k)$ with the output of encoder net $g(x(k))$, the lifting state $\Phi(x(k))$ in (21) can be obtained.

Linear Net: The linear net consists of four subnets, linear net A, linear net B, linear net H, and linear net J, as shown in Fig. 3. These subnets are specifically designed to approximate the matrices A , B , H , and J in (17), respectively. The output of the linear net is expressed as:

$$\Phi(x(k+1)) = W_A \Phi(x(k)) + W_B u(k) + W_H \epsilon(k) + W_J \vartheta(k), \quad (23)$$

where $W_A \in \mathbb{R}^{n_\phi \times n_\phi}$, $W_B \in \mathbb{R}^{n_\phi}$, $W_H \in \mathbb{R}^{n_\phi}$, and $W_J \in \mathbb{R}^{n_\phi}$ represent the weights of linear net A, B, H, and J, respectively. To enhance the efficiency of backpropagation

and accelerate convergence, the biases in all subnets of the linear nets are set to zero.

Decoder Net: The decoder net approximates the matrix C in (17) and reconstructs the original system state from the high-dimensional lifting state. Similar to the linear net, the output of the decoder net is the forward-predicted state, expressed as:

$$x(k+1) = W_C \Phi(x(k+1)), \quad (24)$$

where W_C denotes the weights of the decoder net.

To achieve excellent performance of the DNN, we train the DNN by solving the following optimization problem:

$$\min_{\theta_E, \theta_A, \theta_B, \theta_H, \theta_J, \theta_D} \mathcal{L}, \quad (25)$$

where θ_E , θ_A , θ_B , θ_H , θ_J , and θ_D denote the learning parameters for the encoder net, linear net A, linear net B, linear net H, linear net J, and decoder net, respectively. The loss function \mathcal{L} for learning the DNN parameters is defined as:

$$\mathcal{L} = \alpha_1 \mathcal{L}_p + \alpha_2 \mathcal{L}_l + \alpha_3 \mathcal{L}_r + \alpha_4 \mathcal{L}_e, \quad (26)$$

where α_1 , α_2 , α_3 , and α_4 are weighting coefficients, and \mathcal{L}_p , \mathcal{L}_l , \mathcal{L}_r , and \mathcal{L}_e represent the total prediction loss, linear transform loss, data reconstruction loss, and regularization loss, respectively.

Total Prediction Loss: To ensure accurate prediction of the next step state of the original system, the total prediction loss is defined as:

$$\mathcal{L}_p = \|x(k+1) - x_{\text{true}}(k+1)\|_2^2, \quad (27)$$

where $x_{\text{true}}(k+1)$ represents the true value of the data.

Linear Transform Loss: The linear transform loss is designed to minimize prediction errors in the lifting state space. It quantifies the difference between the predicted lifted state at the next step and the lifting state obtained from the original

system's true state of the next step. This loss function is expressed as:

$$\mathcal{L}_1 = \|\Phi(x(k+1)) - \Phi(x_{\text{true}}(k+1))\|_2^2. \quad (28)$$

Data Reconstruction Loss: In order to minimize the data reconstruction error, the data reconstruction loss is expressed as:

$$\mathcal{L}_r = \|x(k) - W_C \Phi(x(k))\|_2^2. \quad (29)$$

Regularization Loss: To prevent overfitting, a regularization term is incorporated:

$$\mathcal{L}_e = \|\theta_E\|_2^2 + \|\theta_D\|_2^2. \quad (30)$$

Based on the DNN structure and loss functions defined, we train the DNN using pre-collected data (20). In this paper, the training is performed with the Adam optimizer [41]. Upon completion of training, we obtain the matrices A , B , H , J , and C in (17), and the lifting function $\Phi(x(k))$ represented using neural network in (14).

2) *Over-Approximated System Model:* As highlighted in Remark 2, employing the Koopman operator to model the system in (8) with the linear representation in (17) inherently introduces unavoidable modeling errors. Therefore, it is essential to develop a robust control strategy that ensures robustness concerning these errors in (17). To address this challenge, we first formulate an equivalent Koopman lifting system model of (8) that incorporates these modeling errors:

$$\begin{cases} z(k+1) = Az(k) + Bu(k) + H\epsilon(k) + J\vartheta(k) + \sigma(k), \\ x(k) = Cz(k) + \varrho(k), \end{cases} \quad (31)$$

where $\sigma(k)$ and $\varrho(k)$ represent the modeling errors of the Koopman system, arising from a combination of modeling inaccuracies and noise. Motivated by [22], [36], [37], we assume that $\sigma(k)$ and $\varrho(k)$ are bounded by:

$$|\sigma(k)| \leq \sigma_{\max}, \quad |\varrho(k)| \leq \varrho_{\max}, \quad (32)$$

where $\sigma_{\max} \in \mathbb{R}^{n_\phi}$ and $\varrho_{\max} \in \mathbb{R}^{2n}$ denote the bounds for $\sigma(k)$ and $\varrho(k)$, respectively. Techniques for estimating these modeling error boundaries can draw from noise estimation methods, including minimum statistics method [42], Kalman filtering method [43], and Monte Carlo method [44].

To represent the bounded modeling errors in a computationally feasible manner, we transform $\sigma(k)$ and $\varrho(k)$ in (32) into zonotope sets. Specifically, we have:

$$\sigma(k) \in \mathcal{Z}_\sigma, \quad \varrho(k) \in \mathcal{Z}_\varrho, \quad (33)$$

where $\mathcal{Z}_\sigma = \langle c_{\mathcal{Z}_\sigma}, G_{\mathcal{Z}_\sigma} \rangle$ and $\mathcal{Z}_\varrho = \langle c_{\mathcal{Z}_\varrho}, G_{\mathcal{Z}_\varrho} \rangle$ represent zonotope sets for $\sigma(k)$ and $\varrho(k)$, respectively.

For the equivalent Koopman lifting system model in (31), modeling errors may result in multiple possible representations for $[A \ B \ H \ J]$ and C that remain consistent with the data sequences in (20). To account for this uncertainty, we construct matrix zonotope sets $\mathcal{M}_{\text{ABHJ}}$ and \mathcal{M}_C to over-approximate all possible system models $[A \ B \ H \ J]$ and C . The following Lemma 1 establishes the approach for this over-approximation.

Lemma 1: Consider the data sequences U_- , E_- , F_- , X_- , and X_+ in (20) obtained from the mixed vehicle platoon

system (8), along with Z_- and Z_+ in (20) derived from the lifting function $\Phi(x(k))$ in (14) trained via a DNN. Assuming that the matrices $[Z_-^\top \ U_-^\top \ E_-^\top \ F_-^\top]^\top$ and $[Z_-]$ are of full row rank, the sets of all possible matrices $[A \ B \ H \ J]$ and C can be over-approximated as:

$$\mathcal{M}_{\text{ABHJ}} = (Z_+ - \mathcal{M}_\sigma) \begin{bmatrix} Z_- \\ U_- \\ E_- \\ F_- \end{bmatrix}^\dagger, \quad (34)$$

$$\mathcal{M}_C = (X_- - \mathcal{M}_\varrho) [Z_-]^\dagger, \quad (35)$$

where \dagger denotes the Moore–Penrose pseudoinverse of the matrix. The error sets are defined as:

$$\mathcal{M}_\star = \left\langle C_{\mathcal{M}_\star}, \left[G_{\mathcal{M}_\star}^{(1)}, G_{\mathcal{M}_\star}^{(2)}, \dots, G_{\mathcal{M}_\star}^{(\gamma_{\mathcal{M}_\star})} \right] \right\rangle, \quad (36)$$

where \star refers to σ or ϱ , representing the modeling errors. \mathcal{M}_\star is a matrix zonotope set derived from the error zonotope set $\mathcal{Z}_\star = \langle c_{\mathcal{Z}_\star}, G_{\mathcal{Z}_\star} \rangle$, with $G_{\mathcal{Z}_\star} = [g_{\mathcal{Z}_\star}^{(1)}, g_{\mathcal{Z}_\star}^{(2)}, \dots, g_{\mathcal{Z}_\star}^{(\gamma_{\mathcal{Z}_\star})}]$, where $\gamma_{\mathcal{M}_\star} \in \mathbb{N}$ is the number of generator matrices. The specific formulations in (36) are provided as follows:

$$C_{\mathcal{M}_\star} = [c_{\mathcal{Z}_\star} \ \dots \ c_{\mathcal{Z}_\star}], \quad (37a)$$

$$G_{\mathcal{M}_\star}^{(1+(i-1)T)} = \begin{bmatrix} g_{\mathcal{Z}_\star}^{(i)} & 0_{n \times (T-1)} \end{bmatrix}, \quad (37b)$$

$$G_{\mathcal{M}_\star}^{(j+(i-1)T)} = \begin{bmatrix} 0_{n \times (j-1)} & g_{\mathcal{Z}_\star}^{(i)} & 0_{n \times (T-j)} \end{bmatrix}, \quad (37c)$$

$$G_{\mathcal{M}_\star}^{(T+(i-1)T)} = \begin{bmatrix} 0_{n \times (T-1)} & g_{\mathcal{Z}_\star}^{(i)} \end{bmatrix}, \quad (37d)$$

with $\forall i = \{1, 2, \dots, \gamma_{\mathcal{Z}_w}\}$ and $j = \{2, 3, \dots, T-1\}$.

Proof: To simplify the derivations, the sequences of unknown modeling errors are defined as:

$$O_- = [\sigma(1), \sigma(2), \dots, \sigma(T)] \in \mathbb{R}^{n_\phi \times T}, \quad (38)$$

$$\Gamma_- = [\varrho(1), \varrho(2), \dots, \varrho(T)] \in \mathbb{R}^{2n \times T}, \quad (39)$$

although it is important to note that O_- and Γ_- are not directly measurable.

For the equivalent Koopman lifting system model in (31), the following relationships hold:

$$Z_+ = [A \ B \ H \ J] \begin{bmatrix} Z_- \\ U_- \\ E_- \\ F_- \end{bmatrix} + O_-, \quad (40)$$

$$X_- = CZ_- + \Gamma_-. \quad (41)$$

Given that the matrices $[Z_-^\top \ U_-^\top \ E_-^\top \ F_-^\top]^\top$ and $[Z_-]$ are of full row rank, we can derive the following expressions:

$$[A \ B \ H \ J] = (Z_+ - O_-) \begin{bmatrix} Z_- \\ U_- \\ E_- \\ F_- \end{bmatrix}^\dagger, \quad (42)$$

$$C = (X_- - \Gamma_-) [Z_-]^\dagger, \quad (43)$$

where the sequences O_- and Γ_- are unknown, but by applying the corresponding matrix zonotope sets \mathcal{M}_σ and \mathcal{M}_ϱ in (36), we can obtain the matrix zonotope sets $\mathcal{M}_{\text{ABHJ}}$ and \mathcal{M}_C in (34) and (35). These matrix zonotope sets provide an over-approximation of the system models that effectively accounts for the modeling errors. ■

C. Online Control Phase

In the online control phase, we aim to ensure the robustness of the mixed vehicle platoon control against unavoidable modeling errors, external disturbances, and adversarial attacks. To achieve this, we develop the RNDDPC method, which incorporates the Koopman operator and reachability analysis. Initially, we calculate the reachable sets of the system's state over the control horizon, incorporating the effects of these unfavorable factors. To guarantee that the reachable sets remain within the defined safety constraints, we then formulate an optimization problem of the RNDDPC method, which we solve to determine the optimal control inputs for the CAVs.

1) *Data-Driven Reachable Set*: Utilizing the model matrix zonotope sets $\mathcal{M}_{\text{ABHJ}}$ and \mathcal{M}_C derived in (34) and (35), the data-driven reachable set for the state of dynamics in (31) can be determined through Lemma 2.

Lemma 2: Consider the system in (31). Given the trajectories U_- , E_- , F_- , X_- , X_+ , Z_- , and Z_+ , if the matrix $[Z_-^\top U_-^\top E_-^\top F_-^\top]^\top$ and the matrix $[Z_-]$ are of full row rank, the recursive expression for the over-approximated data-driven reachable set is given by:

$$\begin{cases} \hat{\mathcal{R}}^z(i+1|k) = \mathcal{M}_{\text{ABHJ}} \left(\hat{\mathcal{R}}^z(i|k) \times \mathcal{Z}_u \times \mathcal{Z}_\epsilon \times \mathcal{Z}_\vartheta \right) + \mathcal{Z}_\sigma, \\ \hat{\mathcal{R}}(i|k) = \mathcal{M}_C \hat{\mathcal{R}}^z(i|k) + \mathcal{Z}_\varrho, \end{cases} \quad (44)$$

where $\hat{\mathcal{R}}(i|k)$ denotes the over-approximated reachable set for the state $x(i|k)$, and $\hat{\mathcal{R}}^z(i|k)$ represents the over-approximated reachable set for the lifting state $z(i|k)$ of the system (31). The terms \mathcal{Z}_u , \mathcal{Z}_ϵ , \mathcal{Z}_ϑ denote the zonotope sets for control inputs, disturbance inputs, and attack inputs, respectively.

Proof: For the system (31), the state reachable set can be calculated using the following model:

$$\begin{cases} \mathcal{R}^z(i+1|k) = [A \ B \ H \ J] (\mathcal{R}^z(i|k) \times \mathcal{Z}_u \times \mathcal{Z}_\epsilon \times \mathcal{Z}_\vartheta) + \mathcal{Z}_\sigma, \\ \mathcal{R}(i|k) = C \mathcal{R}^z(i|k) + \mathcal{Z}_\varrho, \end{cases} \quad (45)$$

where $[A \ B \ H \ J] \in \mathcal{M}_{\text{ABHJ}}$ and $C \in \mathcal{M}_C$, as stated in Lemma 1. Assuming that $\mathcal{R}^z(i|k)$ and $\hat{\mathcal{R}}^z(i|k)$ originate from the same initial set, it follows that $\mathcal{R}(i|k) \in \hat{\mathcal{R}}(i|k)$. Consequently, the recursive relation in (44) holds, providing an over-approximated reachable set for the system state. ■

2) *RNDDPC Optimization Problem*: This part firstly presents a well-established MPC design framework for mixed vehicle platoon systems (8). While this overview may seem extensive, it aids in understanding our proposed RNDDPC method.

For the nonlinear mixed vehicle platoon system described in (8), a conventional approach is to develop a nonlinear MPC strategy. The primary objective of this controller is to

maintain system stability and ensure safety. The nonlinear MPC controller is formulated as follows.

Nonlinear MPC:

$$\min_{\mathbf{u}(k), \mathbf{x}(k)} \sum_{i=0}^{N-1} (\|x(i|k) - r(i|k)\|_Q^2 + \|u(i|k)\|_R^2) \quad (46a)$$

s.t.

$$x(i+1|k) = f(x(i|k), u(i|k), \epsilon(i|k), \vartheta(i|k)), \quad (46b)$$

$$x(i|k) \in \mathcal{X}, \quad (46c)$$

$$u(i|k) \in \mathcal{U}, \quad (46d)$$

$$\epsilon(i|k) = \epsilon(k), \quad (46e)$$

$$x(0|k) = x(k), \quad (46f)$$

where (46a) represents the cost function, with the optimized variables $\mathbf{u}(k) = \{u(0|k), u(1|k), \dots, u(N-1|k)\}$ and $\mathbf{x}(k) = \{x(0|k), x(1|k), \dots, x(N-1|k)\}$ denoting the sequences of control inputs and predicted states, respectively. The term $r(i|k) = [r_1^\top(k), r_2^\top(k), \dots, r_n^\top(k)]^\top \in \mathbb{R}^{2n}$, with $r_i(k) = [s_i^*(k), v_i^*(k)]^\top$ is the desired state to be tracked at time step $k+i$, and N is the length of the prediction horizon. The weight matrices $Q = \text{diag}(Q_x, \xi Q_x, \dots, \xi^{(n-1)} Q_x) \in \mathbb{R}^{2n \times 2n}$ and $R \in \mathbb{R}$ penalize deviations in states and control inputs, respectively. Specifically, $Q_x = \text{diag}(\rho_s, \rho_v)$ represents the penalty weights for spacing and velocity deviations, with ρ_s and ρ_v are the corresponding weights. The decay factor $0 < \xi \leq 1$ ensures that penalties decrease for HDVs that are further from the CAV.

The (46b) represents the nonlinear dynamics constraints from (8), assuming that attack $\vartheta(i|k)$ and noise $\omega(i|k)$ are zero for online control. The constraint (46c) imposes limits on the system states, where $\mathcal{X} = \{x(k) \in \mathbb{R}^{2n} \mid |x(k) - r(k)| \leq \mathbf{1}_n \otimes \tilde{x}_{\max}\}$. Here, $\tilde{x}_{\max} = [\tilde{s}_{\max}, \tilde{v}_{\max}]^\top$, where \tilde{s}_{\max} and \tilde{v}_{\max} are the constraint limits for spacing and velocity deviations, respectively. Additionally, $\mathbf{1}_n$ is an n dimensional column vector of ones and \otimes denotes the Kronecker product. The (46d) is the control input constraint, we define $\mathcal{U} = \{u(k) \in \mathbb{R} \mid |u(k)| \leq u_{\max}\}$, where u_{\max} defines the maximum control input allowable for the CAVs. The (46e) assumes that the head vehicle is running at a constant velocity $\epsilon(k)$. Finally, the optimization problem is initialized with current state measurement $x(k)$, as shown in constraint (46f).

Notably, the nonlinear dynamics in (46b) can be derived through system identification methods or first-principles modeling. However, accurately modeling the mixed vehicle platoon systems (8), which often involve multiple HDVs, poses significant challenges due to their strong nonlinearities. Consequently, the nonlinear MPC optimization problem in (46) is typically strongly non-convex. Solving these non-convex problems in real time requires substantial computational resources, which can potentially compromise the performance of the nonlinear MPC approach [45]. Moreover, the presence of multiple local minima can undermine control effectiveness, leading to suboptimal strategies. Although linearizing (46b) and employing a linear MPC controller may seem like a viable option, this approach may not adequately capture the inherently nonlinear dynamics of mixed vehicle platoons.

To address the nonlinear challenges inherent in nonlinear MPC framework (46), a promising solution is the Koopman MPC method [26], [27]. This approach replaces the nonlinear dynamics constraints in (46b) with high-dimensional linear dynamics as described by (17). In the Koopman MPC framework, the nonlinear MPC problem (46) is reformulated as a quadratic optimization problem.

Koopman MPC:

$$\min_{\mathbf{u}(k), \mathbf{x}(k)} \sum_{i=0}^{N-1} (\|x(i|k) - r(i|k)\|_Q^2 + \|u(i|k)\|_R^2) \quad (47a)$$

s.t.

$$z(i+1|k) = Az(i|k) + Bu(i|k) + H\epsilon(i|k) + J\vartheta(i|k), \quad (47b)$$

$$x(i|k) = Cz(i|k), \quad (47c)$$

$$x(i|k) \in \mathcal{X}, \quad (47d)$$

$$u(i|k) \in \mathcal{U}, \quad (47e)$$

$$\epsilon(i|k) = \epsilon(k), \quad (47f)$$

$$x(0|k) = x(k), \quad (47g)$$

where the cost function in (47a) is identical to (46a), Similarly, the safety constraints in (47d) and (47e) correspond to those in (46c) and (46d), respectively. However, the dynamics constraints (47b) and (47c) derived from the linear Koopman lifting system model (17), rather than the nonlinear model in (46b). Same as in (46), the attack $\vartheta(i|k)$ and noise $\omega(i|k)$ are assumed to be zero for online control.

For mixed vehicle platoon systems, however, offline data is often corrupted by unknown noise, complicating accurate modeling with the Koopman lifting system model (47b) and (47c). To address this issue, this paper reformulates the problem as a RNDDPC problem using (44). The key idea is to determine the control input $\mathbf{u}(k)$ at each time step k to ensure that the predicted states $\mathbf{x}(k)$ remain within the computed reachable sets, while also keeping these sets within the safety constraints, all while minimizing the associated cost. The RNDDPC problem can be formulated as follows.

RNDDPC:

$$\min_{\mathbf{u}(k), \mathbf{x}(k)} \sum_{i=0}^{N-1} (\|x(i|k) - r(i|k)\|_Q^2 + \|u(i|k)\|_R^2) \quad (48a)$$

s.t.

$$\hat{\mathcal{R}}^z(i+1|k) = \mathcal{M}_{\text{ABHJ}} \left(\hat{\mathcal{R}}^z(i|k) \times \mathcal{Z}_u \times \mathcal{Z}_\epsilon \times \mathcal{Z}_\vartheta \right) + \mathcal{Z}_\sigma, \quad (48b)$$

$$\hat{\mathcal{R}}(i|k) = \mathcal{M}_C \hat{\mathcal{R}}^z(i|k) + \mathcal{Z}_\varrho, \quad (48c)$$

$$\hat{\mathcal{R}}(i|k) \subset \mathcal{X}, \quad (48d)$$

$$x(i|k) \in \hat{\mathcal{R}}(i|k), \quad (48e)$$

$$u(i|k) \in \mathcal{U}, \quad (48f)$$

$$x(0|k) = x(k), \quad (48g)$$

$$\hat{\mathcal{R}}(0|k) = \langle x(k), 0 \rangle, \quad (48h)$$

where $\mathcal{Z}_u = \langle u(i|k), 0 \rangle$, $\mathcal{Z}_\epsilon = \langle \epsilon(k), \epsilon_{\max} \rangle$, and $\mathcal{Z}_\vartheta = \langle 0, \vartheta_{\max} \rangle$, where ϵ_{\max} and ϑ_{\max} represent the bounds for disturbances and attacks, respectively. Constraints (48b) and (48c)

Algorithm 1: RNDDPC

Input: Pre-collected data (U, E, F, X) , system constraints $(\mathcal{X}, \mathcal{U})$, weighting matrices (Q, R) , bounded sets $(\mathcal{Z}_\epsilon, \mathcal{Z}_\vartheta, \mathcal{Z}_\omega)$, control horizon N , and total steps N_s .

- 1 Offline construct data $(U_-, E_-, F_-, X_-, X_+, Z_-, Z_+)$;
- 2 Offline learn the lifting function $\Phi(x(k))$ using DNN;
- 3 Offline calculate \mathcal{Z}_σ and \mathcal{Z}_ϱ by (32) and (33), and learn the matrix zonotope sets $\mathcal{M}_{\text{ABHJ}}$ and \mathcal{M}_C using (34) and (35);
- 4 Initialize the state $x(0)$ at time step 0;
- 5 **while** $0 \leq k \leq N_s$ **do**
- 6 Solve (50) for the optimal control input sequence: $\mathbf{u}(k) = [u^*(0|k), u^*(1|k), \dots, u^*(N-1|k)]$;
- 7 Apply the first control input $u^*(0|k)$ to the CAV;
- 8 Increase the time step $k \leftarrow k+1$ and update the initial state $x(k)$ of the mixed vehicle platoon;
- 9 **end**

are derived from (44). Constraint (48d) ensures that the predicted reachable set $\hat{\mathcal{R}}(i|k)$ satisfies the allowable state constraint \mathcal{X} , while constraint (48e) guarantees that the predicted state sequence $x(i|k)$ remains within the reachable set. Note that the optimization problem (48) is convex.

To implement constraint (48d) and (48e), we need to confirm that the predicted reachable set $\hat{\mathcal{R}}(i|k)$ is a subset of the set \mathcal{X} . To achieve this, we first apply the over-approximation operation in Definition 2 to approximate $\hat{\mathcal{R}}(i|k)$ as an interval set, as outlined in Definition 1:

$$\hat{\mathcal{H}}(i|k) = \text{interval}(\hat{\mathcal{R}}(i|k)) = [\hat{\mathcal{H}}_l(i|k), \hat{\mathcal{H}}_u(i|k)], \quad (49)$$

where $\hat{\mathcal{H}}_l(i|k)$ and $\hat{\mathcal{H}}_u(i|k)$ are defined in (2).

Then, we reformulate (48) to obtain the executable RND-DPC problem as follows:

$$\min_{\mathbf{u}(k), \mathbf{x}(k)} \sum_{i=0}^{N-1} (\|x(i|k) - r(i|k)\|_Q^2 + \|u(i|k)\|_R^2) \quad (50a)$$

s.t.

$$\hat{\mathcal{R}}^z(i+1|k) = \mathcal{M}_{\text{ABHJ}} \left(\hat{\mathcal{R}}^z(i|k) \times \mathcal{Z}_u \times \mathcal{Z}_\epsilon \times \mathcal{Z}_\vartheta \right) + \mathcal{Z}_\sigma, \quad (50b)$$

$$\hat{\mathcal{R}}(i|k) = \mathcal{M}_C \hat{\mathcal{R}}^z(i|k) + \mathcal{Z}_\varrho, \quad (50c)$$

$$\hat{\mathcal{H}}_l(i|k) \geq \mathcal{X}_l, \quad \hat{\mathcal{H}}_u(i|k) \leq \mathcal{X}_u, \quad (50d)$$

$$x(i|k) \geq \hat{\mathcal{H}}_l(i|k), \quad x(i|k) \leq \hat{\mathcal{H}}_u(i|k), \quad (50e)$$

$$u(i|k) \in \mathcal{U}, \quad (50f)$$

$$x(0|k) = x(k), \quad (50g)$$

$$\hat{\mathcal{R}}(0|k) = \langle x(k), 0 \rangle, \quad (50h)$$

where \mathcal{X}_l and \mathcal{X}_u represent the vectors of the lower and upper bounds for each state.

At each time step k , we solve the final RNDDPC optimization problem (50) online using a receding horizon manner. This yields the optimal control input sequence $\mathbf{u}(k) = [u^*(0|k), u^*(1|k), \dots, u^*(N-1|k)]$ and predicted state sequence $\mathbf{x}(k) = [x^*(0|k), x^*(1|k), \dots, x^*(N-1|k)]$. The first

control input $u^*(0|k)$ is then applied to the CAVs. The detailed procedure for the RNDDPC implementation is provided in Algorithm 1.

V. SIMULATION AND RESULTS

In this section, we perform nonlinear simulations to assess the performance of the proposed RNDDPC method in controlling mixed vehicle platoon systems.

A. Simulation Setup

As shown in Fig. 1, the simulation setup considers $n = 3$, representing a platoon composed of one CAV (red) and two HDVs (blue), with a head vehicle (gray) positioned ahead of the platoon. Unlike the simplified point-mass models commonly adopted in studies such as [9], [25], our simulations incorporate vehicles with 2D dynamics (precisely, the Audi A8 model) provided by the PreScan software [46].

For the HDVs ($i \in \Omega_H$) in the simulation, control inputs are modeled using the OVM [12], which is expressed as:

$$u_i(k) = k_{1_i} (V(s_i(k)) - v_i(k)) + k_{2_i} (v_{i-1}(k) - v_i(k)), \quad (51)$$

where k_{1_i} and k_{2_i} are control parameters of the HDVs, and the desired velocity $V(s_i(k))$ is defined as:

$$V(s_i(k)) = \begin{cases} 0, & s_i(k) \leq s_{\min} \\ V_m(s_i(k)), & s_{\min} < s_i(k) < s_{\max} \\ v_{\max}, & s_i(k) \geq s_{\max}, \end{cases} \quad (52)$$

where s_{\min} and s_{\max} represent the minimum and maximum spacings, and v_{\max} is the maximum velocity. The nonlinear desired velocity function $V_m(s_i(k))$ is defined as in [10]:

$$V_m(s_i(k)) = \frac{v_{\max}}{2} \left(1 - \cos \left(\pi \frac{s_i(k) - s_{\min}}{s_{\max} - s_{\min}} \right) \right). \quad (53)$$

In the simulation, the parameters for the HDVs, indexed by $i \in \Omega_H$ in (51)-(53), are set as follows: $k_{1_i} = 0.6$, $k_{2_i} = 0.9$, $v_{\max} = 38$, $s_{\max} = 35$, and $s_{\min} = 5$.

For the CAV ($i \in \Omega_C$) in the simulation, its control input is obtained using the proposed RNDDPC method, with the following simulation parameters:

- For the data collection phase, datasets are collected near a traffic velocity of $v^* = 19$ m/s and are utilized for all subsequent experiments. During this phase, the control input for the CAV employs the OVM model in (51) as a pre-designed controller to facilitate normal driving operations. The head vehicle's velocity is an external disturbance input, modeled as a random fluctuation $\epsilon(k) \sim \mathbb{U}[17, 21]$, where \mathbb{U} denotes the uniform distribution. Additionally, random attack inputs $\vartheta(k) \sim \mathbb{U}[-2, 2]$ and random noise $\omega(k) \sim \mathbf{1}_{2n} \otimes \mathbb{U}[-0.03, 0.03]$ are introduced. To ensure adequate persistent excitation, the offline collected trajectories have a length of $T = 10000$ with a sampling interval of 0.05 s. These trajectories are used to construct the data sequences in (20).
- For the offline learning phase, the collected data is split into training, testing, and validation sets in a 7 : 2 : 1 ratio

for training the DNN that estimates the lifting function. The DNN structure is depicted in Fig. 3, with the encoder net comprising $n_e = 5$ layers with 32, 32, 64, 32, and 16 neurons, respectively, resulting in $n_\phi = 16$ lifting functions. The linear networks for matrices A, B, H, and J consist of layers with 16 neurons each. The decoder net is configured with 6 neurons. Training is performed with a batch size of 128, a learning rate of 0.001, and loss function weights of $\alpha_1 = 1$, $\alpha_2 = 10$, $\alpha_3 = 0.3$, and $\alpha_4 = 0.0001$. The over-approximated system matrix zonotope sets \mathcal{M}_{ABHJ} and \mathcal{M}_C are learned based on (34) and (35), with error bounds $\sigma_{\max} = \mathbf{1}_{n_\phi} \otimes 0.2$ and $\varrho_{\max} = \mathbf{1}_{2n} \otimes 0.3$, as specified in (32).

- For the online control phase, the simulation is performed under attack inputs $\vartheta(k) \sim \mathbb{U}[-3, 3]$ and noise $\omega(k) \sim \mathbf{1}_{2n} \otimes \mathbb{U}[-0.03, 0.03]$. The prediction horizon is set to $N = 3$. The cost function weights in (50a) defined as $\rho_s = 1$, $\rho_v = 1$, $\xi = 0.6$, and $R = 0.1$. State constraints are set as $\tilde{x}_{\max} = [7, 7]^\top$ and $\tilde{x}_{\min} = [7, 10]^\top$ for comprehensive simulations and emergency simulations. Input constraint is set as $u_{\max} = 5$ in (50). The head vehicle's velocity $v_0(k)$ is set to the desired reference velocity $v_i^*(k)$ for each vehicle. For the HDVs, the desired spacing $s_i^*(k)$ is determined by the inverse model $V^{-1}(s_i(k))$ of (52). For the CAV, a constant time headway strategy is adopted, where $s_i^*(k) = t_h \times v_i^*(k) + s_{\min}$, with a time headway of $t_h = 1.2$ s. The disturbance boundary is set to $\epsilon_{\max} = 2$, while the attack boundary is set to $\vartheta_{\max} = 3$. The simulation operates with a time step of 0.05 s.

The simulations are implemented using MATLAB 2024a and PreScan. Optimization problems are formulated with the YALMIP toolbox [47] and solved using the Mosek solver [48]. Reachable sets are computed with the CORA toolbox [49]. All simulations are conducted on a computer equipped with an Intel Core i9-13900KF CPU and 64 GB of RAM.

For comparative analysis, some baseline methods are included:

- 1) The nonlinear MPC (NMPC) method, assumes full knowledge of system dynamics (8) based on (51), but does not account for noise, disturbances, or attacks, as outlined in (46).
- 2) The linear MPC (LMPC) method linearizes the known system dynamics (8) while maintaining the same setup as the nonlinear MPC.
- 3) The Koopman MPC (KMPC) method, as described in [26], [27], utilizes the same lifting function as our proposed method and follows the formulation in (47).
- 4) The DeePC method is implemented based on [9], [17], which does not explicitly consider noise, disturbances, or attacks.
- 5) The ZPC method from [20], [29] employs zonotope sets for data-driven control, explicitly incorporating noise, disturbances, and attacks. The ZPC setup aligns closely with our method, with the primary distinction being its reliance on a linear system assumption.

All baseline methods share identical parameter settings for the cost function (46a) and the safety constraints (46d)

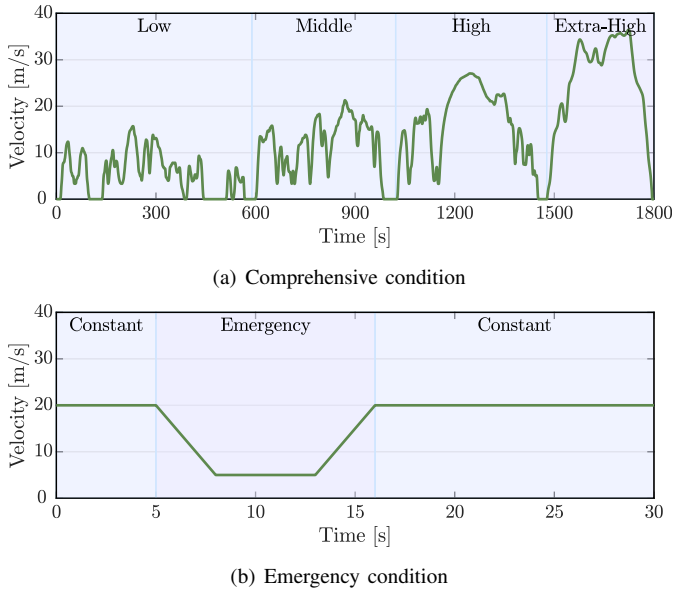


Fig. 4. The velocity profiles for comprehensive simulations and emergency simulations.

and (46f) with RNDDPC, except that ZPC uses a prediction horizon of $N = 3$, while the other methods use $N = 10$. For further contrast, an all-HDV scenario is also included, where the CAV is controlled using the OVM in (51).

After completing the experiments with a total duration of T_s , data from each vehicle is collected for performance evaluation. To quantify the tracking accuracy of the proposed RNDDPC method and the baseline approaches, two performance indices are employed: tracking velocity mean error R_v and tracking spacing mean error R_s , which are defined as follows:

$$R_v = \frac{1}{N_s} \frac{1}{n} \sum_{k=0}^{N_s} \sum_{i=1}^n |v_i(k) - v^*(k)|, \quad (54a)$$

$$R_s = \frac{1}{N_s} \frac{1}{n} \sum_{k=0}^{N_s} \sum_{i=1}^n |s_i(k) - s_i^*(k)|, \quad (54b)$$

where $N_s = T_s/t_s$ represents the total number of simulation steps. In (54a) and (54b), lower values of R_v and R_s indicate better tracking performance of the vehicles in the mixed vehicle platoon relative to the head vehicle, while higher values signify poorer tracking accuracy.

In addition, based on (50a), the total real cost R_c is employed to evaluate the control performance of different methods, as defined by:

$$R_c = \sum_{k=0}^{N_s} (\|x(k) - r(k)\|_Q^2 + \|u(k)\|_R^2), \quad (55)$$

where R_c reflects the overall control efficiency, with smaller values of R_c signifying more efficient control performance.

B. Comprehensive Simulations

Standard driving cycles are commonly employed to evaluate the performance of mixed vehicle platoon control algorithms [9], [20]. In order to evaluate the effectiveness of our method, we employ the Worldwide harmonised Light vehicles

Test Procedure (WLTP) as the simulation condition [50]. The velocity profile of WLTP is shown in Fig. 4(a), which includes low velocity, middle velocity, high velocity, and extra-high velocity phases, covering a variety of driving conditions such as urban, suburban, and highway scenarios.

The simulation results under WLTP are presented in Fig. 5. For clarity, we only visualize the results of all-HDVs, linear MPC, DeePC, and proposed RNDDPC. Here, we focus on analyzing the tracking velocity and inter-vehicle spacing errors within a mixed vehicle platoon consisting of one CAV and two HDVs. Overall, in the presence of noise, disturbances, and attacks, linear MPC in Fig. 5(b) and RNDDPC in Fig. 5(d) demonstrate reduced velocity and spacing errors compared to the all-HDVs scenario. This improvement is attributed to the optimal control frameworks employed by these methods, which enhance tracking performance. In contrast, the DeePC method exhibits the poorest tracking accuracy, as shown in Fig. 5(c). This poor performance is likely due to its reliance on historical trajectory data to construct an online dynamic model. Such reliance makes DeePC vulnerable to noise, disturbance, and attacks, which corrupt the data and undermine its predictive accuracy and control effectiveness.

In addition, a closer examination of Fig. 5(b) and (d) reveals that the red, green, and purple lines corresponding to RNDDPC show lower tracking errors compared to linear MPC. In particular, the tracking error profiles for the CAV, represented by the red line, stand out prominently. This indicates that the proposed RNDDPC outperformed linear MPC in reducing tracking errors for both CAVs and HDVs. The superior performance of RNDDPC is attributed to their ability to capture the nonlinear dynamics of the mixed vehicle platoon system, whereas linear MPC employs a simplified linear predictor. Additionally, RNDDPC utilizes a set-based approach that anticipates noise, disturbance, and attack effects, making it a more robust control strategy. Consequently, our RNDDPC ensures more stable and efficient operation of the mixed vehicle platoon system.

To further quantify the simulation results for our method and all baseline methods, we employ three key performance indices: the tracking velocity mean error R_v , tracking spacing mean error R_s , and total real cost R_c indices, as defined in (54a), (54b), and (55). These metrics allow a comprehensive assessment of the control effectiveness across different methods. As illustrated in Table I, all approaches, except for the DeePC method, outperform the all-HDVs scenario in terms of tracking and control efficiency. Notably, the nonlinear MPC and Koopman MPC methods, which account for the system's nonlinear characteristics, outperform the linear MPC method. This advantage likely stems from their enhanced predictive capabilities regarding the system's future states. Regarding robustness, the ZPC method performs better than other baseline methods when subjected to noise, disturbances, and attacks. It is noteworthy that the proposed RNDDPC method achieves the lowest values across R_v , R_s , and R_c , owing to its careful consideration of nonlinear dynamics and robustness in mixed platoon control. Specifically, compared to the best-performing ZPC method among the baseline approaches, the proposed RNDDPC method still realizes further reductions of 3.6%,

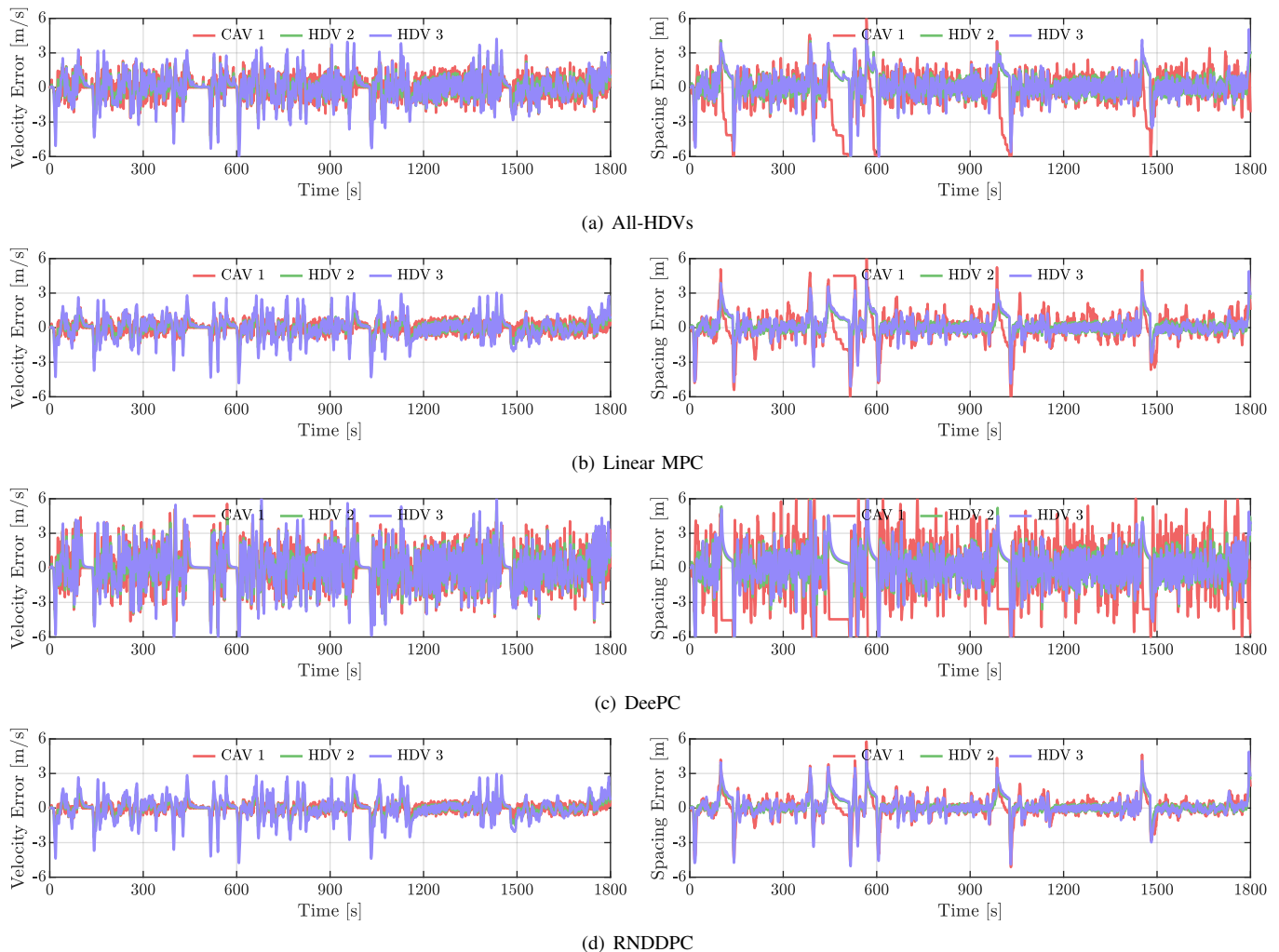


Fig. 5. Tracking velocity and spacing errors in comprehensive simulations for RNDPDC and baseline methods. The red line, the green line, and the purple line represent the CAV (labeled 1), the HDV (labeled 2), and the HDV (labeled 3), respectively. All data-driven control methods use the same dataset.

TABLE I
PERFORMANCE COMPARISON IN COMPREHENSIVE SIMULATIONS

	All HDVs	NMPC	LMPC	KMPC	DeePC	ZPC	RNDPDC
R_v	0.81	0.56	0.57	0.56	1.24	0.55	0.53
R_s	0.95	0.61	0.70	0.62	1.65	0.60	0.57
$R_c (\times 10^5)$	1.28	0.55	0.69	0.57	3.23	0.53	0.51

5.0%, and 3.8% in indices R_v , R_s , and R_c , respectively. These results demonstrate that by employing the Koopman operator to capture the nonlinear characteristics of the mixed vehicle platoon and utilizing the reachable set analysis to proactively address adverse factors such as noise, disturbances, and attacks, our RNDPDC method can significantly improve the tracking control performance of mixed vehicle platoons with nonlinear dynamics in environments where noise, disturbances, and attacks coexist.

C. Emergency Simulations

To thoroughly assess the tracking safety of the proposed RNDPDC method, we conducted a comparative experiment under emergency conditions, as shown in Fig. 4(b). In this scenario, the head vehicle initially travels at a constant velocity of 20 m/s, then applies an abrupt braking maneuver with

a deceleration of -5 m/s^2 for 3s, reducing its velocity to 5 m/s. The head vehicle maintains this reduced velocity for 5s before accelerating at a maximum rate of 5 m/s^2 to return to the original velocity of 20 m/s. The total duration of this emergency scenario is 30s. Simulation results for this emergency event, using different control strategies, are presented in Fig. 6.

In assessing the performance of various control strategies, we employ the same evaluation metrics as in the comprehensive simulations, specifically tracking velocity error and tracking spacing error, to compare the effectiveness of each method. The results reveal that, in the presence of noise, disturbances, and attacks, the all-HDV scheme (see Fig. 6(a)) and the DeePC method (see Fig. 6(c)) exhibit significant tracking errors in both velocity and spacing, indicating a lack of robustness for both approaches. While the linear MPC

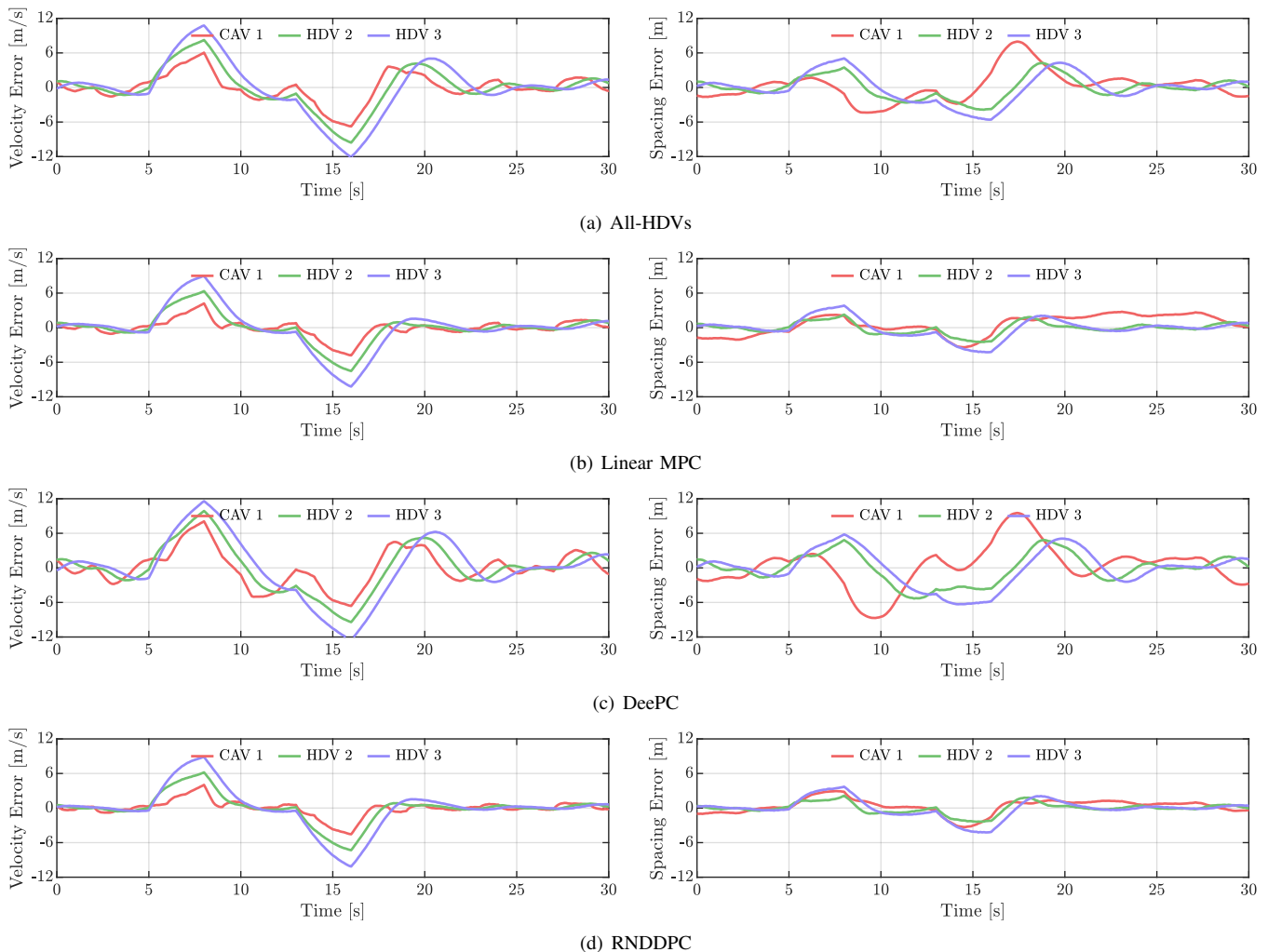


Fig. 6. Tracking velocity and spacing errors in emergency simulations for RNDDPC and baseline methods. The red line, the green line, and the purple line represent the CAV (labeled 1), the HDV (labeled 2), and the HDV (labeled 3), respectively. All data-driven control methods use the same dataset.

TABLE II
PERFORMANCE COMPARISON IN EMERGENCY SIMULATIONS

	All HDVs	NMPC	LMPC	KMPC	DeePC	ZPC	RNDDPC
R_v	2.47	1.54	1.58	1.56	3.09	1.50	1.47
R_s	1.75	0.97	1.17	0.99	2.38	0.96	0.93
$R_c (\times 10^4)$	1.00	0.45	0.49	0.46	1.56	0.44	0.42

performs adequately in controlling velocity error, it exhibits considerable deficiencies in spacing error, particularly between 20s to 30s in Fig. 6(b), underscoring the limitations of linear MPC in controlling mixed vehicle platoons. In contrast, RNDDPC demonstrates superior performance in both tracking velocity and spacing, as illustrated in Fig. 6(d). These findings are consistent with the results observed in the comprehensive simulation scenarios.

Additionally, we assess the three key performance metrics, and the results for each method under emergency conditions are presented in Table II. The analysis reveals that the proposed RNDDPC method outperforms all baseline approaches, yielding the lowest values for R_v , R_s , and R_c . These results highlight the superior robustness and control precision of RNDDPC in emergency scenarios. Furthermore, they underscore the effectiveness of our approach, which leverages the

Koopman operator to model the nonlinear dynamics of the mixed vehicle platoon, while proactively mitigating adverse factors such as noise, disturbances, and attacks through reachability analysis. This confirms the safety performance of our method.

VI. CONCLUSIONS

In this paper, we have proposed a Robust Nonlinear Data-Driven Predictive Control (RNDDPC) method for mixed vehicle platoons. This method explicitly addresses the nonlinear dynamics inherent in mixed vehicle platoons and is designed to ensure robustness against noise, disturbances, and adversarial attacks. To handle the system's nonlinearity, we employ a deep EDMD learning technique that maps the system's nonlinear behavior into a linear representation in a high-dimensional space, providing a more tractable model for control design.

To further enhance model robustness, we introduce an over-approximated matrix zonotope set method, which enables secondary learning to construct a robust linear predictor based on reachable sets, effectively compensating for potential modeling inaccuracies, disturbances, and attacks. By integrating Koopman operator theory with reachability analysis technology, we formulate the RNDDPC optimization problem to achieve robust control, even in the presence of disturbances, noise, and attacks, thus guaranteeing system safety. Compared to existing methods, extensive simulation results demonstrate the superior performance and robustness of the proposed method in mixed vehicle platoon control. Future research will focus on addressing communication delays in mixed vehicle platoon control and conduct real-world experiments to further validate and refine the proposed control framework.

REFERENCES

- [1] H. U. Ahmed, Y. Huang, P. Lu, and R. Bridgelall, "Technology developments and impacts of connected and autonomous vehicles: An overview," *Smart Cities*, vol. 5, no. 1, pp. 382–404, 2022.
- [2] Z. Wang, C. Lv, and F.-Y. Wang, "A new era of intelligent vehicles and intelligent transportation systems: Digital twins and parallel intelligence," *IEEE Transactions on Intelligent Vehicles*, 2023.
- [3] S. Feng, Z. Song, Z. Li, Y. Zhang, and L. Li, "Robust platoon control in mixed traffic flow based on tube model predictive control," *IEEE Transactions on Intelligent Vehicles*, vol. 6, no. 4, pp. 711–722, 2021.
- [4] C. Chen, J. Wang, Q. Xu, J. Wang, and K. Li, "Mixed platoon control of automated and human-driven vehicles at a signalized intersection: dynamical analysis and optimal control," *Transportation research part C: emerging technologies*, vol. 127, p. 103138, 2021.
- [5] T. Liu, L. Cui, B. Pang, and Z.-P. Jiang, "A unified framework for data-driven optimal control of connected vehicles in mixed traffic," *IEEE Transactions on Intelligent Vehicles*, vol. 8, no. 8, pp. 4131–4145, 2023.
- [6] M. Amoozadeh, H. Deng, C.-N. Chuah, H. M. Zhang, and D. Ghosal, "Platoon management with cooperative adaptive cruise control enabled by vanet," *Vehicular communications*, vol. 2, no. 2, pp. 110–123, 2015.
- [7] Y. Zhu, D. Zhao, and H. He, "Synthesis of cooperative adaptive cruise control with feedforward strategies," *IEEE Transactions on Vehicular Technology*, vol. 69, no. 4, pp. 3615–3627, 2020.
- [8] S. Li, H. Zheng, J. Wang, C. Chen, Q. Xu, J. Wang, and K. Li, "Influence of information flow topology and maximum platoon size on mixed traffic stability," *Transportation Research Part C: Emerging Technologies*, vol. 171, p. 104950, 2025.
- [9] J. Wang, Y. Zheng, K. Li, and Q. Xu, "DeeP-LCC: Data-enabled predictive leading cruise control in mixed traffic flow," *IEEE Transactions on Control Systems Technology*, vol. 31, no. 6, pp. 2760–2776, 2023.
- [10] I. G. Jin, S. S. Avedisov, C. R. He, W. B. Qin, M. Sadeghpour, and G. Orosz, "Experimental validation of connected automated vehicle design among human-driven vehicles," *Transportation research part C: emerging technologies*, vol. 91, pp. 335–352, 2018.
- [11] D. Hajdu, I. G. Jin, T. Insperger, and G. Orosz, "Robust design of connected cruise control among human-driven vehicles," *IEEE Transactions on Intelligent Transportation Systems*, vol. 21, no. 2, pp. 749–761, 2019.
- [12] M. Bando, K. Hasebe, A. Nakayama, A. Shibata, and Y. Sugiyama, "Dynamical model of traffic congestion and numerical simulation," *Physical review E*, vol. 51, no. 2, p. 1035, 1995.
- [13] M. Treiber, A. Hennecke, and D. Helbing, "Congested traffic states in empirical observations and microscopic simulations," *Physical review E*, vol. 62, no. 2, p. 1805, 2000.
- [14] Y. Wang, S. Lin, Y. Wang, B. De Schutter, and J. Xu, "Robustness analysis of platoon control for mixed types of vehicles," *IEEE Transactions on Intelligent Transportation Systems*, vol. 24, no. 1, pp. 331–340, 2022.
- [15] C. Zhao and H. Yu, "Enforcing safety for mixed traffic control via a control barrier function quadratic program," *IFAC-PapersOnLine*, vol. 56, no. 2, pp. 2226–2231, 2023.
- [16] J. Berberich, J. Köhler, M. A. Müller, and F. Allgöwer, "Data-driven model predictive control with stability and robustness guarantees," *IEEE Transactions on Automatic Control*, vol. 66, no. 4, pp. 1702–1717, 2020.
- [17] J. Coulson, J. Lygeros, and F. Dörfler, "Data-enabled predictive control: In the shallows of the deepc," in *2019 18th European Control Conference (ECC)*. IEEE, 2019, pp. 307–312.
- [18] D. Li, K. Zhang, H. Dong, Q. Wang, Z. Li, and Z. Song, "Physics-augmented data-enabled predictive control for eco-driving of mixed traffic considering diverse human behaviors," *IEEE Transactions on Control Systems Technology*, 2024.
- [19] K. Zhang, K. Chen, Z. Li, J. Chen, and Y. Zheng, "Privacy-preserving data-enabled predictive leading cruise control in mixed traffic," *IEEE Transactions on Intelligent Transportation Systems*, 2023.
- [20] J. Lan, D. Zhao, and D. Tian, "Data-driven robust predictive control for mixed vehicle platoons using noisy measurement," *IEEE Transactions on Intelligent Transportation Systems*, vol. 24, no. 6, pp. 6586–6596, 2021.
- [21] X. Shang, J. Wang, and Y. Zheng, "Decentralized robust data-driven predictive control for smoothing mixed traffic flow," *IEEE Transactions on Intelligent Transportation Systems*, pp. 1–16, 2024.
- [22] Q. Xu, Y. Liu, J. Pan, J. Wang, J. Wang, and K. Li, "Reachability analysis plus satisfiability modulo theories: An adversary-proof control method for connected and autonomous vehicles," *IEEE Transactions on Industrial Electronics*, vol. 70, no. 3, pp. 2982–2992, 2022.
- [23] J. Guo, H. Guo, J. Liu, D. Cao, and H. Chen, "Distributed data-driven predictive control for hybrid connected vehicle platoons with guaranteed robustness and string stability," *IEEE Internet of Things Journal*, vol. 9, no. 17, pp. 16 308–16 321, 2022.
- [24] M. Lazar, "Basis-functions nonlinear data-enabled predictive control: Consistent and computationally efficient formulations," in *2024 European Control Conference (ECC)*. IEEE, 2024, pp. 888–893.
- [25] J. Zhan, Z. Ma, and L. Zhang, "Data-driven modeling and distributed predictive control of mixed vehicle platoons," *IEEE Transactions on Intelligent Vehicles*, vol. 8, no. 1, pp. 572–582, 2022.
- [26] M. Korda and I. Mezić, "Linear predictors for nonlinear dynamical systems: Koopman operator meets model predictive control," *Automatica*, vol. 93, pp. 149–160, 2018.
- [27] —, "Koopman model predictive control of nonlinear dynamical systems," *The Koopman Operator in Systems and Control: Concepts, Methodologies, and Applications*, pp. 235–255, 2020.
- [28] M. O. Williams, I. G. Kevrekidis, and C. W. Rowley, "A data-driven approximation of the koopman operator: Extending dynamic mode decomposition," *Journal of Nonlinear Science*, vol. 25, pp. 1307–1346, 2015.
- [29] A. Alanwar, Y. Stürz, and K. H. Johansson, "Robust data-driven predictive control using reachability analysis," *European Journal of Control*, vol. 68, p. 100666, 2022.
- [30] A. Alanwar, A. Koch, F. Allgöwer, and K. H. Johansson, "Data-driven reachability analysis from noisy data," *IEEE Transactions on Automatic Control*, 2023.
- [31] M. Althoff, "Reachability analysis and its application to the safety assessment of autonomous cars," Ph.D. dissertation, Technische Universität München, 2010.
- [32] W. Kühn, "Rigorously computed orbits of dynamical systems without the wrapping effect," *Computing*, vol. 61, pp. 47–67, 1998.
- [33] J. Wang, Y. Zheng, C. Chen, Q. Xu, and K. Li, "Leading cruise control in mixed traffic flow: System modeling, controllability, and string stability," *IEEE Transactions on Intelligent Transportation Systems*, vol. 23, no. 8, pp. 12 861–12 876, 2021.
- [34] I. G. Jin and G. Orosz, "Optimal control of connected vehicle systems with communication delay and driver reaction time," *IEEE Transactions on Intelligent Transportation Systems*, vol. 18, no. 8, pp. 2056–2070, 2016.
- [35] J. Wang, X. Li, J. H. Park, and G. Guo, "Distributed mpc-based string stable platoon control of networked vehicle systems," *IEEE Transactions on Intelligent Transportation Systems*, vol. 24, no. 3, pp. 3078–3090, 2022.
- [36] X. Jin, W. M. Haddad, Z.-P. Jiang, and K. G. Vamvoudakis, "Adaptive control for mitigating sensor and actuator attacks in connected autonomous vehicle platoons," in *2018 IEEE Conference on Decision and Control (CDC)*. IEEE, 2018, pp. 2810–2815.
- [37] X. Zhang, W. Pan, R. Scattolini, S. Yu, and X. Xu, "Robust tube-based model predictive control with koopman operators," *Automatica*, vol. 137, p. 110114, 2022.
- [38] M. Han, Z. Li, X. Yin, and X. Yin, "Robust learning and control of time-delay nonlinear systems with deep recurrent koopman operators," *IEEE Transactions on Industrial Informatics*, 2023.
- [39] V. Cibulka, T. Haniš, and M. Hromčík, "Data-driven identification of vehicle dynamics using koopman operator," in *2019 22nd International Conference on Process Control (PC19)*. IEEE, 2019, pp. 167–172.
- [40] Y. Xiao, X. Zhang, X. Xu, X. Liu, and J. Liu, "Deep neural networks with koopman operators for modeling and control of autonomous

- vehicles,” *IEEE transactions on intelligent vehicles*, vol. 8, no. 1, pp. 135–146, 2022.
- [41] D. P. Kingma, “Adam: A method for stochastic optimization,” *arXiv preprint arXiv:1412.6980*, 2014.
- [42] H. Farsi, “Improvement of minimum tracking in minimum statistics noise estimation method,” *Signal Processing: An International Journal (SPIJ)*, vol. 4, no. 1, pp. 17–25, 2010.
- [43] Y. Bulut, D. Vines-Cavanaugh, and D. Bernal, “Process and measurement noise estimation for kalman filtering,” in *Structural Dynamics, Volume 3: Proceedings of the 28th IMAC, A Conference on Structural Dynamics, 2010*. Springer, 2011, pp. 375–386.
- [44] G. Kimaev and L. A. Ricardez-Sandoval, “Multilevel monte carlo for noise estimation in stochastic multiscale systems,” *Chemical Engineering Research and Design*, vol. 140, pp. 33–43, 2018.
- [45] M. Diehl, H. J. Ferreau, and N. Haverbeke, “Efficient numerical methods for nonlinear mpc and moving horizon estimation,” *Nonlinear model predictive control: towards new challenging applications*, pp. 391–417, 2009.
- [46] J. Ortega, H. Lengyel, and Z. Szalay, “Overtaking maneuver scenario building for autonomous vehicles with prescan software,” *Transportation Engineering*, vol. 2, p. 100029, 2020.
- [47] J. Lofberg, “Yalmip: A toolbox for modeling and optimization in matlab,” in *2004 IEEE international conference on robotics and automation (IEEE Cat. No. 04CH37508)*. IEEE, 2004, pp. 284–289.
- [48] M. ApS, “Mosek optimization toolbox for matlab,” *User’s Guide and Reference Manual, Version*, vol. 4, no. 1, 2019.
- [49] M. Althoff, “Guaranteed state estimation in cora 2021,” in *Proc. of the 8th International Workshop on Applied Verification of Continuous and Hybrid Systems*, 2021.
- [50] M. Tutuianu, P. Bonnel, B. Ciuffo, T. Haniu, N. Ichikawa, A. Marotta, J. Pavlovic, and H. Steven, “Development of the world-wide harmonized light duty test cycle (wltc) and a possible pathway for its introduction in the european legislation,” *Transportation research part D: transport and environment*, vol. 40, pp. 61–75, 2015.